Stockholm University

Functional Nanocellulose–Tannin Materials Inspired by Nature and Traditional Processes

Konstantin Kriechbaum

Doctoral Thesis in Materials Chemistry at Stockholm University, Sweden 2020

Functional Nanocellulose–Tannin Materials Inspired by Nature and Traditional Processes

Konstantin Kriechbaum

Academic dissertation for the Degree of Doctor of Philosophy in Materials Chemistry at Stockholm University to be publicly defended on Thursday 29 October 2020 at 13.00 digitally via Zoom. Public link will be made available at https://www.mmk.su.se/

Abstract

Renewable and biodegradable alternatives to fossil-based materials are essential as concerns over depleting finite resources and the pollution of our ecosystems are growing. Abundant, highly anisotropic, and mechanically strong cellulose nanofibrils (CNF) are attractive building blocks for the fabrication of high-performance biobased materials that can compete with their conventional fossil-based counterparts. This thesis presents potential solutions to key challenges in the production and properties of CNF and CNF-based materials, such as low moisture resistance and energy-intense processing, by using the physicochemical properties of tannins. The benchmarking of CNF to improve energy-efficient production was investigated and the ability of plant-derived tannins to precipitate proteins, react with nucleophiles when oxidized, and coordinate to metal ions was exploited to produce multifunctional films and foams that were inspired by Nature or traditional processes.

Wet strong, antioxidant, and UV-blocking CNF-based films were produced by mimicking the traditional process of leather tanning. Oxidized CNF were grafted with gelatin that was precipitated with a water-soluble tannin. The polyphenolic tannin provided the films with good radical scavenging properties and efficient blocking of light in the UV-B/UV-C range. The insoluble gelatin–tannin complexes conferred upon the material wet mechanical properties that were comparable to the dry mechanical performance of fossil-based packaging films. So far, there is no universally accepted approach to account for how the swelling of a hygroscopic CNF-based film influences its mechanical properties in humid or wet conditions. Here, a best practice for determining and reporting wet strength is suggested.

Inspired by the sclerotization of insect cuticle, a scalable route towards moisture-resilient, strong, and thermally insulating CNF-based foams was developed. The CNF were modified with a polyamine, ice-templated, treated with an oxidized tannin, solvent-exchanged to ethanol, and evaporatively dried. The cross-linked structure had a high compressive modulus and a thermal conductivity close to that of air, even at high relative humidities.

A method to produce micron-sized patterns on CNF films based on the traditional *Bògòlanfini* dyeing technique is presented. The films were pre-impregnated with a tannin and patterned using microcontact printing with a metal-salt-soaked stamp. The line and dot patterns were analyzed and their colors were tuned by changing the metal ion in the printing ink or the pH.

The final part of the thesis describes a novel approach to assess the degree of CNF fibrillation during energy-efficient grinding by analyzing the structure and properties of anisotropic foams. The optimal energy input during fiber disintegration that produced CNF foams with the best mechanical and thermal insulation properties, as well as the highest CNF and foam cell wall orientation, was identified.

Keywords: *Cellulose, Nanofibrils, Tannin, Biobased, Films, Foams, Moisture resistance, Energy efficiency.*

Stockholm 2020
http://urn.kb.se/resolve?urn=urn:nbn:se:su:diva-185022

ISBN 978-91-7911-296-7
ISBN 978-91-7911-297-4

Department of Materials and Environmental Chemistry (MMK)

Stockholm University, 106 91 Stockholm

Stockholm University

FUNCTIONAL NANOCELLULOSE–TANNIN MATERIALS INSPIRED BY NATURE AND TRADITIONAL PROCESSES

Konstantin Kriechbaum

Stockholm University

Functional Nanocellulose–Tannin Materials Inspired by Nature and Traditional Processes

Konstantin Kriechbaum

ISBN print 978-91-7911-296-7
ISBN PDF 978-91-7911-297-4

The cover image is a photograph of my home region, the Austrian *Weinviertel* ("wine quarter"), which was taken by my father.

Printed in Sweden by Universitetsservice US-AB, Stockholm 2020

To Linnéa, Emil, my
sister, and my parents

Doctoral Thesis 2020

Department of Materials and Environmental Chemistry
Stockholm University
SE-106 91 Stockholm, Sweden

Faculty opponent

Prof. Alain Dufresne

Laboratory of Pulp and Paper Science and Graphic Arts, LGP2
Grenoble Institute of Technology, Grenoble, France

Evaluation committee

Prof. Monica Ek
Department of Fibre and Polymer Technology
KTH Royal Institute of Technology, Stockholm, Sweden

Prof. Belén Martín-Matute
Department of Organic Chemistry
Stockholm University, Stockholm, Sweden

Docent Daniel Söderberg
Department of Mechanics
KTH Royal Institute of Technology, Stockholm, Sweden

Substitute

Prof. Arnold Maliniak
Department of Materials and Environmental Chemistry
Stockholm University, Stockholm, Sweden

Abstract

Renewable and biodegradable alternatives to fossil-based materials are essential as concerns over depleting finite resources and the pollution of our ecosystems are growing. Abundant, highly anisotropic, and mechanically strong cellulose nanofibrils (CNF) are attractive building blocks for the fabrication of high-performance biobased materials that can compete with their conventional fossil-based counterparts. This thesis presents potential solutions to key challenges in the production and properties of CNF and CNF-based materials, such as low moisture resistance and energy-intense processing, by using the physicochemical properties of tannins. The benchmarking of CNF to improve energy-efficient production was investigated and the ability of plant-derived tannins to precipitate proteins, react with nucleophiles when oxidized, and coordinate to metal ions was exploited to produce multifunctional films and foams that were inspired by Nature or traditional processes.

Wet strong, antioxidant, and UV-blocking CNF-based films were produced by mimicking the traditional process of leather tanning. Oxidized CNF were grafted with gelatin that was precipitated with a water-soluble tannin. The polyphenolic tannin provided the films with good radical scavenging properties and efficient blocking of light in the UV-B/UV-C range. The insoluble gelatin–tannin complexes conferred upon the material wet mechanical properties that were comparable to the dry mechanical performance of fossil-based packaging films. So far, there is no universally accepted approach to account for how the swelling of a hygroscopic CNF-based film influences its mechanical properties in humid or wet conditions. Here, a best practice for determining and reporting wet strength is suggested.

Inspired by the sclerotization of insect cuticle, a scalable route towards moisture-resilient, strong, and thermally insulating CNF-based foams was developed. The CNF were modified with a polyamine, ice-templated, treated with an oxidized tannin, solvent-exchanged to ethanol, and evaporatively dried. The cross-linked structure had a high compressive modulus and a thermal conductivity close to that of air, even at high relative humidities.

A method to produce micron-sized patterns on CNF films based on the traditional *Bògòlanfini* dyeing technique is presented. The films were pre-impregnated with a tannin and patterned using microcontact printing with a metal-salt-soaked stamp. The line and dot patterns were analyzed and their colors were tuned by changing the metal ion in the printing ink or the pH.

The final part of the thesis describes a novel approach to assess the degree of CNF fibrillation during energy-efficient grinding by analyzing the structure and properties of anisotropic foams. The optimal energy input during fiber disintegration that produced CNF foams with the best mechanical and thermal insulation properties, as well as the highest CNF and foam cell wall orientation, was identified.

List of publications

This thesis is based on the following publications:

I. Antioxidant and UV-Blocking Leather-Inspired Nanocellulose-Based Films with High Wet Strength

Konstantin Kriechbaum and Lennart Bergström
Biomacromolecules, **2020,** 21 (5), 1720–1728.

II. Sclerotization-inspired aminoquinone cross-linking of thermally insulating and moisture-resilient bio-based foams

Konstantin Kriechbaum, Varvara Apostolopoulou-Kalkavoura, Pierre Munier, and Lennart Bergström
Manuscript in preparation

III. Functionalization and patterning of nanocellulose films by surface-bound nanoparticles of hydrolyzable tannins and multivalent metal ions

Mukta V. Limaye, Christina Schütz, Konstantin Kriechbaum, Jakob Wohlert, Zoltán Bacsik, Malin Wohlert, Wei Xia, Mama Pléa, Cheick Dembele, German Salazar-Alvarez, and Lennart Bergström
Nanoscale, **2019**, 11 (41), 19278–19284.

IV. Best Practice for Reporting Wet Mechanical Properties of Nanocellulose-based Materials

Andreas Walther, Francisco Lossada, Tobias Benselfelt, Konstantin Kriechbaum, Lars Berglund, Olli Ikkala, Tsuguyuki Saito, Lars Wågberg, and Lennart Bergström
Biomacromolecules, **2020**, 21 (6), 2536–2540.

V. Analysis of the Porous Architecture and Properties of Anisotropic Nanocellulose Foams: A Novel Approach to Assess the Quality of Cellulose Nanofibrils (CNFs)

Konstantin Kriechbaum, Pierre Munier, Varvara Apostolopoulou-Kalkavoura, and Nathalie Lavoine
ACS Sustainable Chemistry & Engineering, **2018**, 6 (9), 11959–11967.

My contributions to the above listed publications are:

I. Performed all of the experimental work and prepared the manuscript.

II. Performed most of the experimental work and prepared the manuscript.

III. Performed all patterning experiments and prepared parts of the manuscript.

IV. Contributed to the literature research and preparation of the manuscript.

V. Performed most of the experimental work and prepared the manuscript.

Contents

List of abbreviations

AFM	Atomic force microscopy
bPEI	Branched polyethylenimine
CNF	Cellulose nanofibrils
CNC	Cellulose nanocrystals
CP-MAS	Cross-polarization magic-angle spinning
DACNF	Dialdehyde cellulose nanofibrils
DI	Deionized (water)
DPPH	2,2-diphenyl-1-picrylhydrazyl
EA	Ellagic acid
EDX	Energy-dispersive X-ray
FT-IR	Fourier-transform infrared
GA	Gallic acid
NMR	Nuclear magnetic resonance
PDMS	Polydimethylsiloxane
RH	Relative humidity
SDS	Sodium dodecyl sulfate
SEM	Scanning electron microscopy
TA	Tannic acid
TEA	Triethanolamine
TEMPO	(2,2,6,6-Tetramethylpiperidin-1-yl)oxyl
T-CNF	TEMPO-oxidized cellulose nanofibrils
UV-Vis	Ultraviolet-visible
XRD	X-ray diffraction

1 Introduction

Starting from the early 20th century, materials based on fossil-derived plastics have progressively replaced natural materials due to their low cost and appealing properties. They have not just significantly transformed material science, but became an integral part of our daily lives with a global production of ~359 million tons in 2018.[1] However, the resulting dependence on finite resources combined with the significant environmental damage caused by the production and poor recycling of non-biodegradable plastics is a critical problem of our time. In addition, the pollution of our ecosystem with microplastics and their subsequent accumulation in many organisms is a major concern that led to a ban on certain single-use plastics in the EU in 2019.[2,3] Driven by concerns like these, material science has shifted towards finding renewable and biodegradable alternatives whose performance can compete with conventional fossil-based materials. Biopolymers, such as the polysaccharides cellulose, chitin, and alginate, as well as polypeptides and polyphenols, represent more sustainable, abundant, and biodegradable substitutes for fossil-derived polymers. Cellulose is considered a particularly promising sustainable substitute since it is already produced industrially on a large scale for e.g. paper products or textile fibers, and is the most abundant polymer on Earth. The polysaccharide is found among others in higher plants, algae, bacteria, fungi, and animals, and consists of a linear chain of β(1→4)-linked anhydro-D-glucose units.[4] The hydroxyl groups on its backbone enable the water-insoluble chains to assemble via intramolecular and intermolecular hydrogen bonding.[5] The resulting stacked polymer chains form an anisotropic semi-crystalline structure in four main polymorphs Cellulose I–IV, and Cellulose I is most abundant form in Nature. Cellulose is secreted by enzymes that polymerize glucose as elementary fibrils that are 3–4 nm in width and >1 μm in length and made up of rod-like cellulose nanocrystals (CNC) and disordered regions.[6] Elementary fibrils are further assembled into larger units with widths ranging from 20–50 nm and the term cellulose nanofibrils (CNF) refers to both the assemblies and the elementary fibrils themselves.[7] Trees congregate CNF in microfibrils embed-

ded in a matrix rich in the aromatic polymer lignin and the branched polysaccharide hemicellulose, which confer the load-bearing cell walls with high tensile strength. Depending on the species, wood consists of 40–50% cellulose, 25–35% hemicelluloses, and 25–35% lignin, and the hierarchical structure of wood spans over several length scales (Figure 1.1).[8]

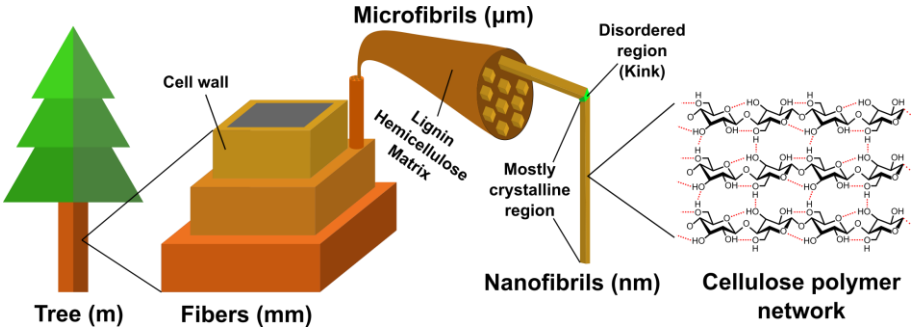

Figure 1.1. The hierarchical structure of wood ranges over several orders of magnitude.

The grand challenge that both the industry and the scientific community face, however, is to make renewable cellulose-based materials that match or even supersede the performance of the fossil-based materials they aim to replace. Nanosized cellulose particles are an auspicious solution to this challenge due to the intriguing physical and chemical properties that result from their small size. Colloidal suspensions of cellulose nanocrystals (CNC), produced by acid hydrolysis of wood cellulose, were reported in the early 1950s[9] and cellulose nanofibrils (CNF), produced from homogenizing wood pulp, were first described in 1983.[10] A recent societal effort to find novel uses for wood, combined with progress in process development, has put the spotlight back on nanocelluloses. The longer and more flexible CNF entangle and form a strong network, whereas the rod-like and stiff CNC can self-assemble and show birefringence. Here, for the production of flexible and mechanically resilient nanocellulose-based materials, CNF were the material of choice.

1.1. CNF: Isolation, properties and applications

CNF have been obtained from many cellulosic sources, such as agricultural residues, annual plants, or sludge but the main industrial source for cellulose and CNF is wood.[11,12] The wood pulp is usually chemically treated to remove most of the lignin and hemicelluloses e.g. via the Kraft or Sulfite processes. The pulp fibers are mechanically disintegrated in a top-down process where high enough shear forces break apart the strong interfibrillar interactions and promote the separation of CNF from larger aggregates.[13] The energy needed for this disintegration step can be significantly lowered by using chemical[14–17] or enzymatic[18] pretreatments. During the TEMPO-mediated oxidation of cellulose fibers, for example, hydroxyl groups on the glucose C6 carbon are selectively oxidized to carboxyl groups.[14] As a result of increased electrostatic repulsion, gentle mechanical disintegration is sufficient to produce highly individualized CNF. However, pretreatment steps pose high environmental impacts, rely on expensive or harmful chemicals that hinder large scale production, or change the CNF surface chemistry.[19,20] The main methods for mechanical disintegration include homogenization, microfluidization, and grinding, but alternative techniques, such as cryocrushing, extrusion, high-intensity ultrasonication, aqueous counter collision, ball milling, steam explosion, or twin-screw extrusion have also been reported.[21] Following intensive research efforts, CNF production has reached commercial scale[22] and it is estimated that the world market for nanosized cellulose particles will grow from 2020 annually over 20% to reach 783 million dollars by 2025.[23]

Once produced, CNF stand out as sustainable bio-nanomaterials with excellent mechanical properties, such as a specific strength and stiffness superior to those of most glasses, plastics, ceramics, metals, and alloys.[24] Further advantages of CNF include their abundance, renewability, low density (1.60 kg m^{-3}),[25] non-toxicity, low thermal expansion coefficient ($<5 \times 10^{-6}$ K^{-1}),[26] and biodegradability.[27] Moreover, the abundant hydroxyl groups on the surface of the CNF allow for targeted modifications to tailor the CNF properties and add functionalities.[5] The potential applications of CNF include, the use as reinforcement in polymer composites, as rheological modifier and stabilizer in food products, coatings, and inks, as a strengthening agent in paper, board, and coatings, to improve the mechanical and barrier properties of packaging films, to make flexible, lightweight, and transparent electronics, and as biocompatible building block in biomedical application.[28,29]

1.2. CNF-based materials

CNF are usually isolated in aqueous environments and processed as dilute suspensions. Thus, dewatering and drying are crucial steps in the production of CNF-based materials. The alignment and packing of the anisotropic fibrils can be tuned by controlling the process parameters (e.g. counterions, pH, or the addition of polymers) and drying methods, resulting in materials with designed CNF morphology and physical properties. Hence, the CNF building blocks can be assembled into novel functional bulk materials, such as beads, hydrogels, continuous fibers, films/coatings, or foams/aerogels via bottom-up techniques.[30] Self-standing films and foams have been reported in the papers included in this thesis and will be discussed in more detail.

Self-standing CNF-based films, also called nanopapers, can be produced by casting, filtering, hot-pressing or spin-coating, among which the dewatering of CNF suspensions through casting or filtration are the main methods (Figure 1.2a). During casting, the solvent slowly evaporates and the concentration of CNF increases homogeneously until interfibril interactions lead to aggregation. The vacuum-assisted filtration of CNF suspensions, on the other hand, leads to dense packing of CNF at the interface between the suspension and the filtration membrane. Both methods can take several hours to form a film, which represents a bottleneck towards a large-scale industrial production. To avoid warping and cracking caused by inhomogeneous drying, the almost-dry films are usually pressed or dried at elevated RH in a final step. The micrometer-thin and layered films (Figure 1.2b) display excellent mechanical properties, high oxygen-barrier properties, optical transparency, and low thermal expansion at low humidity.[31–33] The mechanical performance of CNF-based films has been extensively studied and is influenced by many parameters, including the processing method, humidity, fibril type (e.g. different origin, isolation route, surface chemistry, crystallinity, aspect ratio, degree of polymerization), fibril alignment, porosity, suspension chemistry (e.g. change of counter-ion or pH), or the addition of polymers or inorganic particles.[24] Films can further be functionalized either by the incorporation of an additive to the initial CNF suspension, or by chemically modifying the CNF itself. CNF-based films are being considered as a green alternatives to fossil-based films in applications such as water purification or packaging.[32,34,35]

CNF are also a suitable candidate for the production of ultralight, flexible and strong foams or aerogels with high specific surface areas for applications such as biomedical scaffolds, electrical devices, and high-performance thermal insulation.[36] CNF-based porous materials are sometimes called foams or aerogels. Although the nomenclature is somewhat flexible, the porosity in aerogels is primarily within the mesoporous ($2 \leq$ pore size ≤ 50 nm) range, whereas foams are mainly macroporous (pore size > 50 nm).[36] Structural collapse due to capillary-pressure-induced stresses during the evaporation of water is usually overcome by supercritical or freeze-drying the wet foams or hydrogels (Figure 1.2c). Supercritical drying involves exchanging the water in an aqueous gel with a supercritical fluid (commonly CO_2 after an intermediate solvent exchange step) that can be sublimed into gas without surface tension and capillary stress. Freeze-drying is preceded by either isotropic or anisotropic freezing of the wet gel. During directional ice-templating, also called freeze-casting, ice crystals that grow along a temperature gradient push aside CNF particles, resulting in an anisotropic structure (Figure 1.2d). Sublimation of the ice gives a structure in which the columnar or lamellar macropores or cells are aligned in the freezing direction (Figure 1.2e). The resulting foams or aerogels can have densities as low as 1 kg m^{-3} (porosity >99%) depending on the solid content in the initial suspension and specific surface areas up to 600 m^2 g^{-1}, as well as high specific mechanical properties and low thermal conductivities that outperform fossil-based foams at low or moderate relative humidities.[37–39]

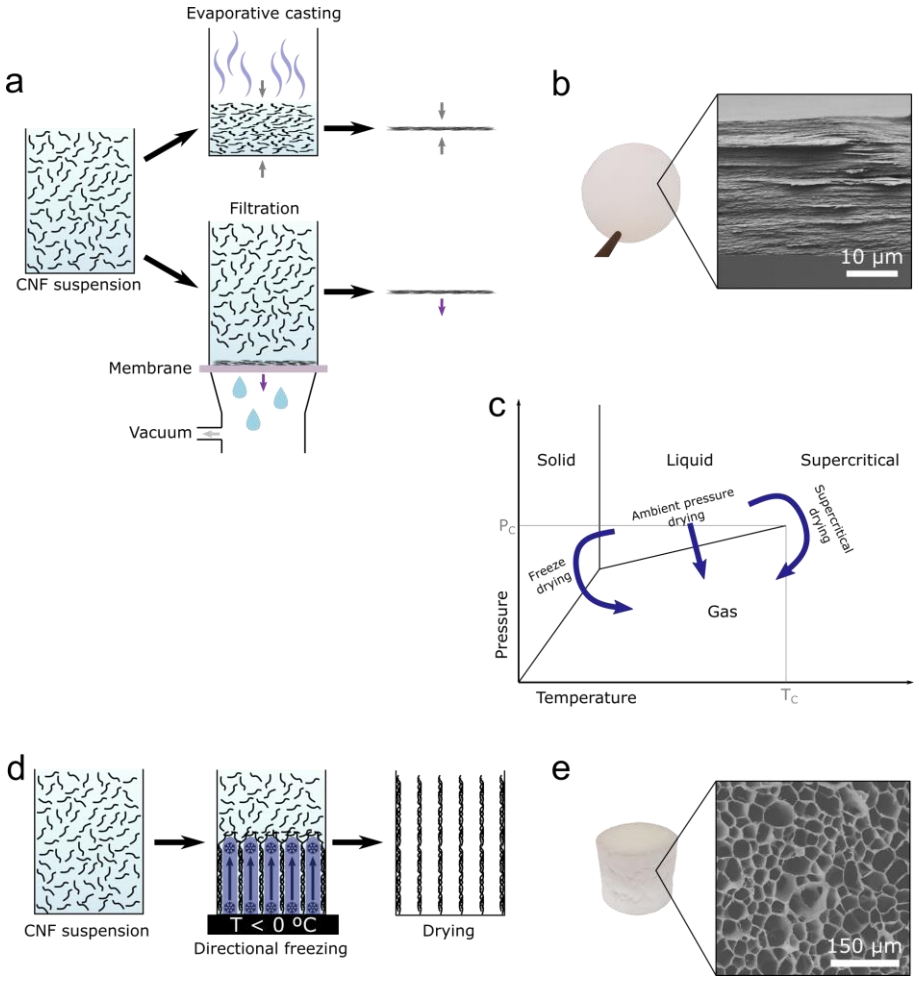

Figure 1.2. Schematic illustration of (a) CNF film preparation via evaporative casting or vacuum filtration that results in (b) a self-standing film showing a layered cross-sectional structure. (c) A hypothetical phase diagram showing the different drying techniques; and (d) the process of directional ice-templating of a CNF suspensions that results in a dried foam with (e) a honeycomb structure in its radial direction.

1.3. Key challenges for the production and properties of CNF and CNF-based materials

As the interest of researchers and companies in CNF as a versatile and bio-based high-performance material continues to grow, there are some major issues that need to be addressed before CNF can reach their full potential.

1.3.1. Resilience of films and foams in humid and wet conditions

The inherent hydrophilicity of cellulose causes CNF-based materials to easily absorb water, which results in a substantial reduction in their strength and barrier properties as well as an increase in thermal conductivity in humid and wet conditions.[40,41] Thus, decreasing the sensitivity of CNF-based films and foams to water is a key challenge for reaching the full potential of CNF in certain applications. The water uptake and swelling of films made from CNF is significantly higher compared to conventional paper made from macroscopic cellulose fibers, as the surface area increases with decreasing particle size.[40] The sensitivity to swelling is further linked to the surface chemistry and crystallinity of CNF, as charged groups increase the water uptake due to the additional osmotic swelling pressure and as water penetrates more easily into the disordered rather than the crystalline regions of cellulose.[42,43] Several strategies have been suggested to chemically or physically crosslink or hydrophobize CNF-based materials to increase their water resilience and wet mechanical properties.[44,45] Finding additional environmentally friendly routes to increase the water resistance of CNF-based materials while maintaining their biodegradability is crucial for certain replacing fossil-based materials.

1.3.2. Evaporative drying methods for foams

Super-insulating CNF-based foams (i.e. those with thermal conductivity below that of air) have been proposed as potential alternatives to fossil-based thermal insulation[39,46,47] and it is crucial to preserve the original network structure of the material after drying. During evaporative drying of hydrogels, the small pore sizes and high surface tension of water lead to a high negative hydrostatic pressure. The network of hydrophilic CNF can usually not withstand these high capillary forces, which results in the densification, shrinkage or collapse of the structure. Thus, ultrahigh porosities and nanosized pores are usually achieved by freeze-drying or supercritical drying of aqueous nanocellulose-based gels or wet foams.[36] However, these processes are energy- and

time-intensive, require batch processing, are difficult to scale up, and rely on expensive equipment.[48,49] Energy-efficient evaporative drying in an oven is a well-established industrial process and could enable a more sustainable mass production of CNF-based foams or aerogels. In order to prevent structural collapse or deformation caused by the hydrostatic pressure during the evaporation of water, a CNF-based gel or wet foam needs to be stabilized and often solvent-exchanged to a low-surface-tension solvent. Previous strategies to strengthen the aqueous CNF network to obtain isotropic evaporatively dried CNF foams and aerogels include non-covalent[50–53] or covalent crosslinking.[54,55]

1.3.3. Functionalization using sustainable components

Materials based on CNF can be considered as sustainable due to the renewable origin of CNF. However, a true transition from fossil-based to fully sustainable materials requires that the components used to tune the properties of CNF-based materials are also eco-friendly. Examples of CNF-based hybrid materials that incorporate different biopolymers include strong fibers with spider silk proteins,[56] water resistant films with chitosan[57] or algal polysaccharides,[58] or biocompatible composites with collagen.[59] Wood, in particular, is an important bioresource not just for cellulose, but also for components that can improve the performance of CNF-based materials. These include for example hemicelluloses that reinforce hydrogels[60] or lignin that renders films more ductile and water resistant.[61] Residues from the forestry industry, such as tree bark that is removed during production and usually burnt for energy recovery, constitute an important source for extractives.[62] Examples of components that can be extracted from bark include monomers of suberin, which have been used to hydrophobize CNC-containing films,[63] non-cellulosic polysaccharides, and tannins. The latter can make up a substantial fraction of the bark, depending on the plant species, and is an underutilized renewable resource for the production of materials or aromatic chemicals.[64] Recently, CNF has been mixed with tannin to prepare antioxidant and UV-blocking thin films.[65,66]

1.3.4. CNF production: Energy efficiency and quality benchmarking

The high energy consumption and associated cost required to generate high shear forces that promote fiber delamination is a major obstacle in the commercialization of CNF. Grinding the fibers between one static and one rotating disc is considered the most energy efficient method for fibrillation, compared to common high-pressure homogenization, as it does not require any form of pretreatment and has the highest production capacity.[67] The degree of fibrillation of a CNF sample is a component of its quality, and thus must be measureable. Microscopic analysis of the CNF morphology are commonly used to study the extent of fibrillation, but the method is not optimal since only a small fraction of a CNF batch is analyzed and large fibers are often excluded due to high magnification. Optical methods that analyze a CNF suspension on several length scales have been suggested,[68] and the degree of fibrillation has been investigated extensively with different characterization techniques or a combination of methods.[69] Recently, the first approach to a universal CNF quality index was proposed; the measurement involved directly investigating the CNF suspended in water and indirectly evaluating the properties of CNF films formed from the suspension.[70] Two multifactor quality indices were suggested; these were based on either eight or four tests that used standard equipment. Measuring the degree of fibrillation of CNF suspensions will not just allow for proper trade and safety assessments, but also help to increase energy-efficiency during production.

1.4. Tannins: Background, properties and applications

Tannins are polyphenolic molecules that accumulate in plants, for example, as defense against predators or as protection against harmful UV radiation.[71] Tannins have been used by mankind for millennia and their ability to precipitate proteins has e.g. been exploited to convert animal hides into leather in a process known as vegetable tanning.[72] Tannins in wine are responsible for its signature astringency as they precipitate salivary proteins and thus reduce lubrication.[73] There are two main classes of tannins: hydrolyzable tannins (Figure 1.3), which are esters of usually glucose and gallic acid, and condensed tannins, which are polymers of flavonoids and are also called proanthocyanidins. Tannins are the second most-abundant natural phenolic material, after

lignin, and can be obtained from the leaves or bark of many trees via solvent or hot-water extraction.[74] These generally water-soluble molecules can form both hydrogen bonds through their abundant polar phenol groups, and hydrophobic π-stacking interactions with their planar aromatic structures. The catechol groups form colored metal-catechol chelate complexes, and this reaction was used to produce iron-gall inks, an important writing ink that was extensively used for more than 300 years.[75] The ability of tannins to stabilize radicals in their phenolic structure results in antioxidant properties and they can, once oxidized, readily react with nucleophiles.[76] Owing to their intriguing properties and biological origin, tannins are nowadays applied in e.g. leather manufacturing, adhesives, food additives, and pharmaceutical applications.[77]

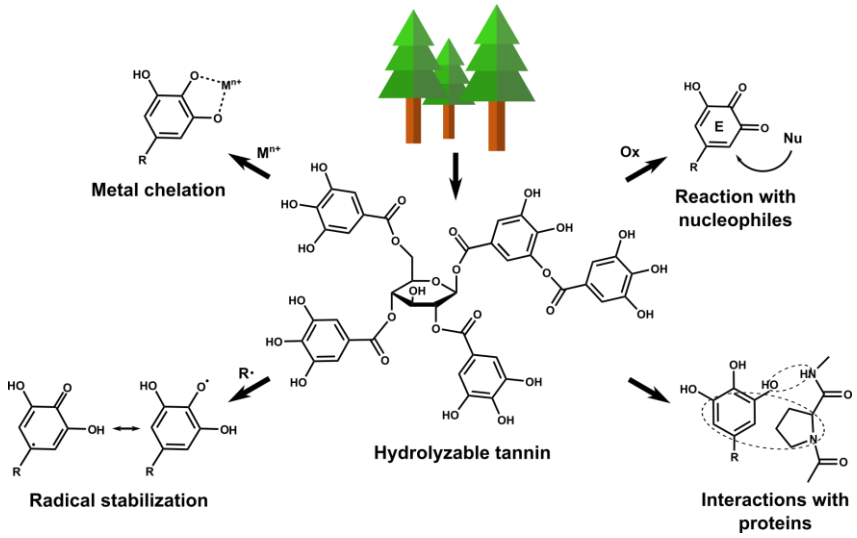

Figure 1.3. Physicochemical properties of a representative plant-derived hydrolyzable tannin.

1.5. Scope of the thesis

The principal motivation for this study is our society's need to find innovative renewable and biodegradable alternatives to fossil-based materials. The materials presented in this thesis are based on cellulose nanofibrils (CNF), a versatile and abundant raw material that is increasingly used in both research and industry for the production of sustainable high-performance materials.

Remaining challenges for CNF-based materials such as their weakening in humid and wet conditions are addressed by using tannins in a leather-inspired and a sclerotization-inspired route towards water resilient films and foams, respectively. The first strategy (Chapter 3, based on paper I) uses the polyphenolic tannin to precipitate gelatin that was grafted onto oxidized CNF. The formation of insoluble gelatin-tannin complexes confers the multifunctional material with wet strength, as well as antioxidant and UV-blocking properties. The lack of a universally accepted best practice when measuring and reporting wet mechanical properties is discussed and a set of recommendations is proposed (Chapter 2.4.3, based on paper IV). During the second route (Chapter 4, based on paper II), the ability of the oxidized tannin to react with nucleophiles is exploited to cross-link an amine-modified CNF network. The resulting moisture-resilient and lightweight foams were both strong and thermally insulating at high relative humidities. The quinone-tanned material withstood evaporative drying with minimal structural change, which is an important requirement for the large-scale production of CNF-based porous materials.

Furthermore, the ability of the tannins to form colored complexes with metal ions is exploited to form tunable micron-sized patterns on CNF films using a method that is based on the traditional *Bògòlanfini* dyeing technique (Chapter 5, based on paper III). A primary consideration in all studies was to use other biobased and safe components and processing routes to modify the CNF-based materials in order to present truly sustainable alternatives to fossil-based materials.

The final part of the thesis (Chapter 6, based on paper V) investigates a new approach to increase the energy efficiency during CNF production by assessing the degree of CNF fibrillation via the analysis of anisotropic foams.

2 Preparation and characterization of materials

More detailed information on the procedures can be found in papers I–V attached.

2.1. CNF preparation

CNF from purely mechanical fibrillation

The CNF described in papers I & V were produced by mechanical fibrillation of never-dried bleached Sulfite (Domsjö Fabriker AB, Sweden) and Kraft (SCA Östrand, Sweden) softwood pulps after washing with 0.5 M HCl, ion-exchanging to the sodium form with 10^{-3} M $NaHCO_3$, and rinsing with DI water until the pH was neutral. The cellulose, hemicelluloses, and lignin contents of the washed pulps (see paper V) were determined by MoRe Research (Örnsköldsvik, Sweden). Initial suspensions of Kraft and Sulfite pulps at a solid content of 2 wt% were dispersed in DI water with a High-Shear Dispermix (Ystral GmbH, Germany). The dispersions were mechanically fibrillated using a supermasscolloider grinder (model MKZA10-15J, Disk model MKE 10-46#, Masuko Sangyo Co. Ltd., Japan). Operating power was used as the unique parameter to control the grinding process. Thus, the rotation rate of the grinding discs was held constant at 750 rpm and the gap between discs was adapted to reach a constant operating power surplus (operating power minus no-load power) of 0.2 kW. The CNF suspensions were circulated through the grinder until the desired energy consumption (kWh, i.e. operating power surplus multiplied by time) was reached. The specific energy consumption (kWh kg^{-1}) for each CNF suspension was calculated by dividing the energy consumption by the initial dry weight of CNF in the suspension.

Preparation of dialdehyde CNF (DACNF)

In paper I, a suspension of mechanically fibrillated Kraft pulp CNF was oxidized to dialdehyde CNF (DACNF) by adding $NaIO_4$ at a ratio $m(NaIO_4):m(CNF_{dry}) = 1:1$. The mixture was stirred for 4 hours at room temperature in an aluminum-foil-wrapped beaker to prevent light-induced decomposition of $NaIO_4$. The periodate was removed after oxidation by washing the suspension with deionized water until the conductivity of the filtrate was below 5 μS cm^{-1} and the final DACNF suspension was stored at 4 °C until use.

Preparation of Gelatin@DACNF

In paper II, 250 mg gelatin (type B) added to 250 mL of a 3 mg mL^{-1} DACNF suspension at 60 °C. The pH was adjusted to 6.5 with 0.1 M NaOH and the mixture was stirred for 3 hours at 60 °C.

Preparation of carboxylated CNF

In papers II & III, carboxylated CNF were produced from never-dried Sulfite softwood pulp (Domsjö Fabriker AB, Sweden) that was oxidized via a TEMPO-mediated oxidation according to a previously reported procedure.[14] After washing, the oxidized pulp was suspended and diluted in DI water and mechanically fibrillated by passing it through a microfluidizer (M-110EH, Microfluidics) at high pressure. The total charge density of the surface-functionalized CNF was determined by conductometric titration to be 1.1 (Paper II) and 0.6 (Paper III) mmol carboxyl groups per gram pulp, respectively.[78]

CNF-based suspensions were prepared by adding DI water and/or additives, mixing with a high-speed disperser (Ultra-Turrax, IKA, Germany) and degassing using centrifugation or vacuum.

2.2. Preparation and patterning of films

CNF-based films were prepared in paper I via vacuum filtration. 15 g of a 3 mg mL^{-1} CNF, DACNF, or Gelatin@DACNF suspension was filtered with vacuum assistance through nylon membranes (GVS, 0.45 μm, hydrophilic), rinsed and dried between paper sheets under a weight at room temperature. The leather-inspired tanning of films in paper I was performed by immersing Gelatin@DACNF films in a solution of 10 mg mL^{-1} TA in DI water for 24 hours before washing with DI water and drying as described above.

In paper III, CNF films were prepared by allowing water to evaporate from 0.2 mL of a 1.5 mg mL^{-1} carboxylated CNF suspension on a flat silicon substrate at room temperature. The films were then impregnated with 10 µL of an aqueous TA or GA solution and dried again. PDMS stamps were prepared from a silicon elastomer kit (Sylgard 184, Dow corning, USA) by replica molding of a silicon master with sub-micron surface features. The pre-impregnated films were patterned by placing PDMS stamps that were saturated with 0.1 M Fe^{3+}, Co^{2+}, and Cu^{2+} aqueous metal salt solutions onto the pre-impregnated films.

2.3. Preparation of foams

Foams were produced by directional ice-templating, also called freeze-casting, and either freeze-drying (papers II & V) or solvent exchange and evaporative drying (paper II). A certain amount of suspension with at least 5 mg mL^{-1} CNF was poured into a polymer mold that was equipped with a copper bottom plate. The mold was then placed onto a block of dry ice (–78.5 °C) until the directional freezing of the suspension was complete. Freeze-drying of the frozen suspension was performed by placing them for at least 72 hours in a freeze-dryer (Alpha 1-2 LDplus, Christ, Germany).

Evaporative-drying (paper II) was achieved by thawing frozen CNF/bPEI suspension in 20 vol% ethanol, increasing the ethanol content (20/40/60/80/99.5 vol%) for solvent exchange, then heating in an oven at 10 °C/hour to 105 °C and holding for 12 hours. The sclerotization-inspired cross-linking was performed by thawing 3 g of the frozen CNF/bPEI suspensions for 20 minutes in 70 mL of a solution of 10 mg mL^{-1} TA in 0.1 M pH 7 sodium phosphate buffer that had been oxidized with 5 mg mL^{-1} $NaIO_4$ immediately before immersing the frozen freeze-cast suspensions. The cross-linked hydrogels were then washed, solvent exchanged to ethanol and dried in an oven as described above.

2.4. Characterization methods

2.4.1. Microscopy

Scanning electron microscopy (SEM) & energy-dispersive X-ray spectroscopy (EDX)

High-resolution SEM and EDX were performed on a JEOL JSM-7401F (JEOL Ltd., Japan) microscope. The morphology of CNF in paper V was observed after drying a drop of 0.01 mg mL^{-1} CNF suspension on a flat glass disc overnight at room temperature and coating with a thin layer of gold. The structure of the cross-section of films in paper I was observed after swelling the film strips in DI water for one hour, crash-freezing, cryo-fracturing, and freeze-drying. Images were taken using an accelerating voltage of 2 kV at a working distance of 8 mm. The elemental composition of the printed patterns on CNF films in paper III was determined using a Link system AN 10000 EDX detector. High-resolution images of foam walls in paper II were taken at an accelerating voltage of 1 kV and a working distance of 8 mm. The porous architecture of cryo-fractured and freeze-dried foams in papers II & V was investigated using a tabletop TM 3000 (Hitachi High Tech, Japan) microscope using an accelerating voltage of 5 kV. The elemental composition of the foam cell wall in paper II was analyzed using the built-in EDX detector.

Optical microscopy

Optical microscopy images of printed patterns in paper III and film cross-sections in paper I were taken on a Eclipse FN1 optical microscope (Nikon, Japan) that was equipped with a 50× objective (WD = 17 mm, NA = 0.45) and a CCD camera (Kappa Zelos-02150C GV, Kappa Optronics GmbH) for capturing digital images. The white balance and contrast of the images were corrected after capture.

Atomic force microscopy (AFM)

Topographical AFM images of CNF in paper II and printed patterns in paper III were obtained on a Dimension 2100 SPM (Veeco/Bruker, USA) in tapping mode. Fibrils were imaged after depositing a drop of 0.01 mg mL^{-1} CNF suspension onto a freshly cleaved mica substrate and drying under ambient conditions. CNF diameters were estimated by performing manual height measurements on at least 80 particles. Patterns were imaged directly on films that were casted onto flat silicon substrates.

2.4.2. Spectroscopy

Fourier-transform infrared spectroscopy (FT-IR)

FT-IR spectra were recorded on a Varian 610-IR spectrometer that was equipped with an ATR detection device with a single reflection diamond element. A measurement was performed by accumulating 32 scans in the spectral region of 4000–400 cm^{-1} with a spectral resolution of 4 cm^{-1}.

Ultraviolet–visible spectroscopy (UV-Vis)

UV-Vis absorbance of CNF-based films in paper I and suspensions in paper II was measured using quartz cuvettes on a Genesys 150 (Thermo Fisher Scientific, USA) or a Lambda 19 (Perkin Elmer, USA) UV-Visible spectrometer in the range of 200–800 nm using air or water, respectively, as background.

Nuclear magnetic resonance spectroscopy (NMR)

In paper II, $^{1}H \rightarrow ^{13}C$ cross-polarization magic-angle spinning (CP-MAS) NMR spectra of dry CNF-based foams were recorded on an Avance-III NMR spectrometer (Bruker, USA) at a magnetic field strength of 14.1 T (Larmor frequencies of 600.1 for ^{1}H and 150.9 MHz for ^{13}C). 4.0 mm zirconia rotors were used and spun on the magic angle at 14.00 kHz. Acquisitions involved a 4 μs proton 90° excitation pulse and matched spin-lock fields that obeyed a modified Hartmann-Hahn condition. The contact time was set to 500 μs and SPINAL-64 proton decoupling at 60 kHz was used. During each measurement 32768 signal transients with 2 s relaxation delays were collected and chemical shifts were referenced with respect to neat tetramethylsilane (TMS).

2.4.3. Mechanical testing in the dry and wet state (Paper IV)

Mechanical testing was performed on an Instron 5966 or 5944 universal testing machine (Instron, USA) that was equipped with a 100 N or 500 N load cell, respectively. The tests were conducted at 23 °C and 50% RH.

Tensile testing

In paper I, the mechanical properties of 20 × 3 mm^2 rectangular film specimens were analyzed using tensile testing in the dry state, after conditioning at 23 °C and 50% RH for at least 48 hours before testing, and in the wet state, after immersion in DI water, simulated seawater, or an aqueous TEA/SDS solution for 1 hour before testing. The gauge length and strain rate were set to 10 mm and 1 mm min^{-1}, respectively, and the thickness of the dry specimens was determined with a digimatic micrometer (Mitutoyo, Japan, accuracy 0.1 μm). The thickness of the wet specimens was calculated by multiplying the dry thickness with a swelling ratio that was determined from optical microscopy images of dry and swollen films. The resulting stress–strain curves were used to determine the Young's modulus as the slope of the initial linear elastic region, the toughness as the area under the curve, and the tensile strength and strain at failure from the point of fracture. A representative stress–strain curve from tensile testing is presented in Figure 2.1a.

Compression testing

The mechanical performance of foams in papers II & V was determined using compression testing after conditioning the foams at 23 °C and 50% or 98% RH for at least 48 hours before testing. The strain rate during compression was set to 10% min^{-1}. The dimensions of the foams were determined with a digital caliper. The CNF foams behaved like cellular solids during compression, with an initial elastic region that is followed by a plastic region where cell walls first collapse and then densify.[79] The Young's modulus, compressive strength, and toughness or energy absorption were determined from the stress–strain curves (Figure 2.1b) as the slope of the initial linear elastic region, the stress at 10% strain, and the area under the curve up to 70% strain, respectively.

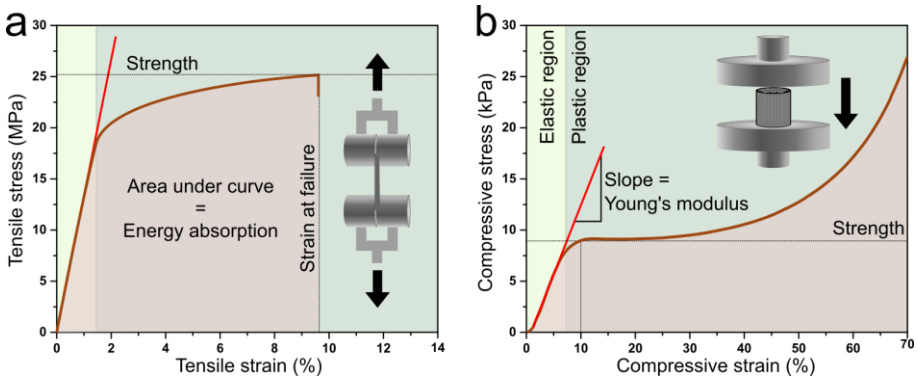

Figure 2.1. Representative stress–strain curves from (a) tensile and (b) compression testing showing how mechanical properties were determined.

Measuring and reporting mechanical properties of wet CNF-based films

The adsorption of water along densely packed hydrophilic surfaces causes CNF-based films to take up substantial amounts of water in humid and wet conditions (Figure 2.2a). CNF are usually packed with an in-plane orientation in vacuum-filtrated or suspension-cast films, thus adsorbed water leads primarily to an increase in film thickness. The larger cross-section of the swollen films results in a lower true stress (σ), which is defined as the force (F) per unit area (A) (Figure 2.2b). Hence, using the dry thickness of films when reporting the wet mechanical properties leads to a critical overestimation of stress-dependent parameters, such as tensile strength and stiffness. Plotting representative stress–strain curves of a hypothetical, but realistic CNF-based film using the correct thickness at a certain water content visualizes the drastic differences in strength (Figure 2.2c).

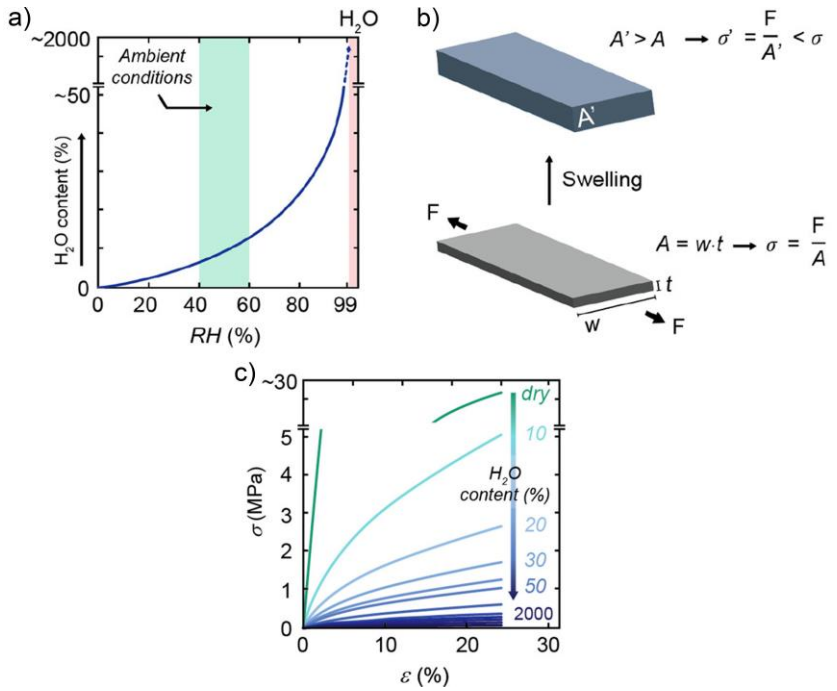

Figure 2.2. Influence of humid and wet conditions on typical hydrophilic nanocellulose-based films: (a) The water content increases with increasing RH, resulting in (b) a swelling-induced expansion of the cross-sectional area of the film that leads to (c) a reduction in stress with increasing water content. Adapted from paper IV.[45] © 2020, Biomacromolecules.

The growing interest in CNF-based films for commercial applications has led to an increasing number of reports on wet mechanical properties (Table 1 in paper IV). However, many studies do not report if or how the swollen thickness of the films was determined, or they directly use the dry thickness for the calculation of wet stress. The different approaches might be caused by the different backgrounds of the researchers determining and reporting the wet mechanical properties. In paper science, for instance, dry dimensions are commonly used for the calculation of the wet strength (e.g., standard SCAN-P 20:95; TAPPI Test Method T 456). Researchers working on the wet mechanical properties of nanocellulose- or other hygroscopic biopolymer-based film would greatly benefit from a common set of recommendations that enables them to benchmark the properties of their material against others. The following core recommendations, which are taken from paper

IV,[45] present a suggested best practice for reporting wet mechanical properties of nanocellulose-based materials.

Core recommendations (taken from paper IV[45]):

1. *The experimental section should clearly state how the evaluation of the mechanical properties at high RH and/or for fully hydrated state was performed, including how the wet dimensions were measured.*
2. *The cross-sectional area in the swollen state should be measured and used for the evaluation. Care needs to be taken when using a caliper to not compress the softened materials excessively. This can be balanced using a flat sheet caliper or placing a coverslip on the soft materials. Additionally, microscopy setups can be used. Values for the thickness of such films may also be estimated from the swelling data at the given humidity or in the wet state, but swelling and deswelling may not always lead to the same dimensions. Hence, measuring the true cross section is advised.*

2.4.4. Other

Thermal gravimetric analysis

The thermal decomposition behavior of the films in paper I was determined on a Discovery TG (TA instruments, USA) by heating approximately 10 mg of film sample to 600 °C at a heating rate of 10 °C min^{-1} in a 40 mL min^{-1} nitrogen flow.

Rheology

The rheological properties of CNF-based suspension in paper II were investigated using a Physica MCR 301 rheometer (Anton Paar, Austria) equipped with a smooth cone-on-plate geometry (2° nominal angle, 25 mm diameter, 50 μm gap) performing amplitude sweeps from 0.01 to 1000% strain at a frequency of 1 Hz and a temperature of 25 °C.

Antioxidant activity

The antioxidant capacity of CNF-based films in paper I was determined using a modified DPPH (2,2-diphenyl-1-picrylhydrazyl) radical scavenging assay.[80] 10 mg of dry film were suspended in 1 mL of 0.1 mM DPPH in methanol and placed in the dark for either 5 min or 5 hours. The absorbance of the

supernatant at 517 nm was then measured using an UV-Vis spectrometer and the DPPH radical scavenging activity was calculated according to equation (1):

$$\text{DPPH inhibition [\%]} = \left(\frac{A_{ref} - A}{A_{ref}}\right) \times 100 \quad (1)$$

where A is the absorbance of the sample supernatant and A_{ref} is the absorbance of 0.1 mM DPPH in methanol.

Ninhydrin assay

The amount of primary amino groups before and after modification of dry CNF-based films in paper I and foams in paper II was determined with a modified Ninhydrin (2,2-dihydroxyindane-1,3-dione) assay.[81] A dry piece of a film or foam specimen was suspended in ethanol, 1 mL of 1.5 % (w/v in ethanol) Ninhydrin solution was added and the suspension was heated to 80 °C for 25 (paper I) or 45 min (paper II). After cooling down, the supernatant was diluted with DI water and its absorbance at 570 nm was measured with a UV-Vis spectrometer against a blank Ninhydrin solution. The absorbance at 570 nm is proportional to the concentration of free primary amino groups.[82]

Sedimentation

The aspect ratio of CNF produced in paper V was determined from sedimentation experiments on 55 mL of 0.150, 0.125, 0.100, 0.075, and 0.050 wt% CNF suspensions using the crowding number theory.[83,84] The ratio of the height of the sediment after one week of sedimentation over the height of the whole suspension was plotted against the initial solid concentration and fit with a quadratic function. The solids concentration at the gel point g_c (kg m^{-3}) corresponds to the linear term of the quadratic function and can be used to calculate the aspect ratio A according to equation (2):

$$A = \frac{6}{\sqrt{\frac{g_c \rho_f}{\rho_l}}} \quad (2)$$

where ρ_l and ρ_f are the densities of water (1000 kg m^{-3}) and cellulose (1500 kg m^{-3}), respectively, and it is assumed that the CNF are perfect cylinders with uniform cross-sections.

Orientation index from image analysis

In paper V, the degree of CNF and cell wall orientation was calculated from SEM images of the foams in the axial direction by using the ImageJ plug-in OrientationJ.[85] The software plots a histogram of the local orientation of every pixel after calculating the structure tensor in its local neighborhood.[86] The resulting histograms were fit with Gaussian curves and an orientation index f was calculated from the full width at half maximum (fwhm) according to equation (3):

$$f = \frac{180 - \text{fwhm}}{180} \tag{3}$$

Degree of CNF alignment from XRD

In papers II & V, the degree of CNF alignment inside the foam walls was determined by X-ray diffraction. 2D patterns of the foams in the radial direction were recorded and an azimuthal integration of the cellulose (200) peak (2θ = 22.6°) was performed. The Hermans' orientation parameter f_H, which can be used to quantify the alignment of CNF in the freezing direction, was calculated according to equation (4):

$$f_H = \frac{3\left(\frac{\sum_0^{\frac{\pi}{2}} I(\varphi)\sin\varphi\cos^2\varphi}{\sum_0^{\frac{\pi}{2}} I(\varphi)\sin\varphi}\right) - 1}{2} \tag{4}$$

where φ is the theoretical angle between the predominant direction CNF and the direction of growing ice crystals during freezing and I(φ) is the intensity at a certain angle φ.[87,88]

Nitrogen sorption

Nitrogen sorption measurements on the foams in papers II & V were performed on an ASAP 2020 (Micromeritics Instrument Corporation, USA) after degassing at 80 °C for 10 hours. The surface area and average pore sizes of the foam walls were estimated using the Brunauer–Emmett–Teller (BET) and the Barrett–Joyner–Halenda (BJH) models, respectively.[89,90]

Density and porosity

In papers II & V, the apparent densities of the foams ρ_{foam} were determined by measuring their volume with a digital caliper and their weight with an analytical balance (Sartorius, Germany) after conditioning for at least 48 hours at 23 °C and either 50% or 98% RH. Their porosity φ was calculated from ρ_{foam} and the skeletal density of the dry foams ρ_{sk}, which was defined as the weighted arithmetic mean of the densities of the components, according to equation (5):

$$\varphi\ [\%] = \left(\frac{1 - \rho_{foam}}{\rho_{sk}}\right) \times 100 \qquad (5)$$

Water uptake

The water uptake of films in paper I was determined by measuring their weight on an analytical balance before and after immersion in DI water. The excess water on wet specimens was removed by blotting with filter paper.

In paper II, the water uptake of foams was determined by measuring the mass change with an analytical balance after conditioning at 20/35/50/65/80% RH inside a Climacell Evo humidity chamber (MMM group, Germany) or at 98% RH after conditioning over a saturated solution of potassium sulfate at 23 °C.

Thermal conductivity

The thermal conductivity of foams in papers II & V was determined with a TPS 2500 S Thermal Constants Analyzer (Hot Disk AB, Sweden) in anisotropic mode.[41] The thermal conductivities in the radial (λ_r) and axial (λ_a) direction of foams were measured in a customized cell at 22 °C and between 5–80% RH. The RH was controlled using a P2 humidifier (Cellkraft, Sweden). For calculations, the dry specific heat capacity of the foams was determined using differential scanning calorimetry on a DSC 1 STARe (Mettler Toledo, USA), where 10 mg of dried material were analyzed between –20 and 50 °C at a 10 °C min^{-1} heating and cooling rate. The wet specific heat capacity at each RH was calculated from the dry one using the water uptake data and the rule of mixtures. The thermal conductivity anisotropy ratio was calculated by dividing λ_a by λ_r.

3 Leather-inspired CNF-based films with high wet-strength (Paper I)

There have been attempts to improve the wet strength of CNF-based films either by the formation of covalent bonds[91–94] or non-covalent interactions.[57,58,95] Unfortunately, there is no standard method to take into account the influence of swelling when measuring and reporting wet mechanical properties, which makes it hard to compare different modification strategies. Besides efforts to enhance water stability, a trend towards active food packaging has sparked research on CNF-based films that are antioxidant and block UV-light.[65,66,96–98]

We designed leather-inspired CNF-based films modified with insoluble gelatin–tannin complexes, which conferred wet strength (paper I). The polyphenolic nature of the incorporated tannin rendered the films antioxidant and UV-blocking.

3.1. Preparation and characterization of films

The preparation of films was inspired by the vegetable tanning of leather, where tannins form insoluble complexes with proteins and transform the putrescible skin into a microbial-resistant and moisture-stabilized material.[99,100] Hence, CNF that was produced by grinding, was oxidized to form dialdehyde-modified CNF (DACNF, 0.78 ± 0.02 mmol aldehyde per gram CNF) and grafted with gelatin, a mixture of peptides and proteins derived from bovine skin collagen, to form Gelatin@DACNF. A dilute suspension of Gelatin@DACNF (Figure 3.1a) was subjected to vacuum filtration (Figure 3.1b) to prepare translucent Gelatin@DACNF films (Figure 3.1c). The dry films were then treated in an aqueous solution of TA (Figure 3.1d), washed, and dried to form the slightly brown and translucent TA/Gelatin@DACNF hybrid films (Figure 3.1e). The network was physically cross-linked by the hydrogen

bonding and hydrophobic interactions that formed between gelatin and TA (Figure 3.1f).

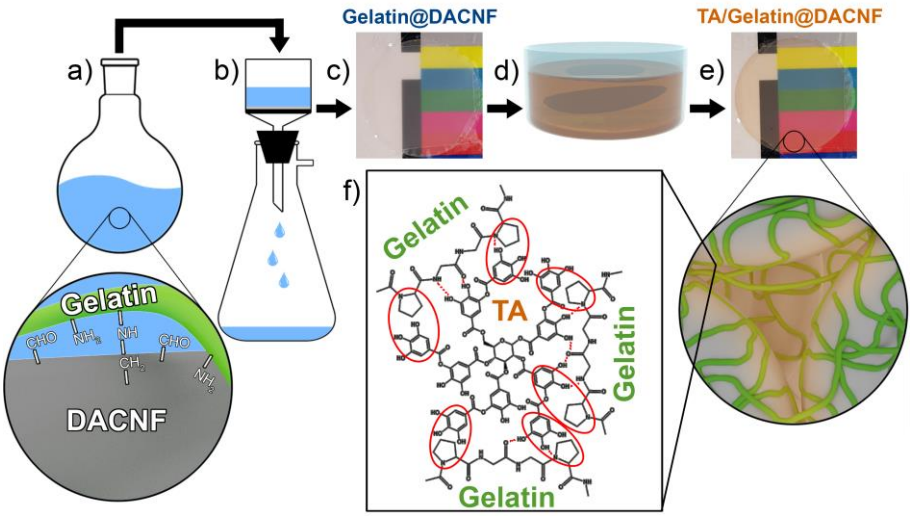

Figure 3.1. Preparation route of the leather-inspired TA/Gelatin@DACNF films: An aqueous suspension of (a) gelatin-grafted DACNF is (b) vacuum-filtrated to form (c) translucent Gelatin@DACNF films that are immersed in an (d) aqueous TA solution to form (e) the slightly brownish leather-inspired TA/Gelatin@DACNF films, in which (f) gelatin and TA are connected by hydrogen bonding and hydrophobic interactions. Taken from paper I.[101] © 2020, Biomacromolecules.

The grafting of gelatin onto DACNF resulted in a gelatin content of 5.9 wt% in the dry Gelatin@DACNF films, which is significantly higher than in vacuum filtered films of physical mixtures of CNF and gelatin (3.7 wt%). The Maillard-type reaction between DACNF aldehydes and gelatin amines reduced the aldehyde content of the DACNF by 29% after grafting of gelatin, as determined from hydroxylamine hydrochloride titration.[102] No further decrease in aldehyde content was observed when increasing the grafting reaction time, which was assigned to the fact that the remaining aldehyde groups are located inside the fibrils and thus not available to react with gelatin.[103] The reduction in surface aldehyde groups could be observed by treating the films

with diamminesilver(I) (Tollens' reagent), where much less bright silver nanoparticles from the reaction with aldehydes could be observed on Gelatin@DACNF films, compared to non-grafted DACNF films (Figure 3.2a). Infrared spectroscopy confirms the absence of the characteristic aldehyde band (1740 cm^{-1}) and the emergence of gelatin amide I, II, and III bands (1637, 1525, and 1259 cm^{-1}, respectively) in the spectra of the grafted Gelatin@DACNF films (Figure 3.2b). In addition, the grafting reaction with DACNF led to a 57% reduction in gelatin primary amine groups, as determined from a modified Ninhydrin colorimetric assay.

The complexation of Gelatin@DACNF films with an aqueous solution of TA led to slightly brown and translucent TA/Gelatin@DACNF films with a final composition of 83.5 ± 0.5 wt% DACNF, 5.2 ± 0.7 wt% gelatin, and 11.2 ± 0.4 wt% TA. Three times more tannin could be incorporated in films that were grafted with gelatin (11.2 wt%), compared to neat CNF films (3.7 wt%). The increase in tannin content suggests the formation of insoluble gelatin-TA complexes in addition to the TA that has been adsorbed onto cellulose.[104] Infrared spectroscopy on TA/Gelatin@DACNF films showed characteristic bands for tannin carbonyl (1700 cm^{-1}) and phenolic (1608 cm^{-1}) groups (Figure 3.2b).

Upon soaking in DI water for 1 hour, the neat CNF films and films of physical mixtures of CNF and gelatin (CNF/Gelatin) swelled significantly, with weight increases of 168 and 141%, respectively (Figure 3.2c). The complexation of gelatin in physical mixtures of CNF and gelatin (CNF/Gelatin/TA) decreased the water uptake to 92%, which is still much higher compared to DACNF (40%) and Gelatin@DACNF (44%) films, where interfibril hemiacetal linkages consolidate the network.[105] The leather-inspired TA/Gelatin@DACNF films had the lowest water uptake of only 25%, which was attributed to the formation of insoluble gelatin–TA complexes that cross-link the structure.

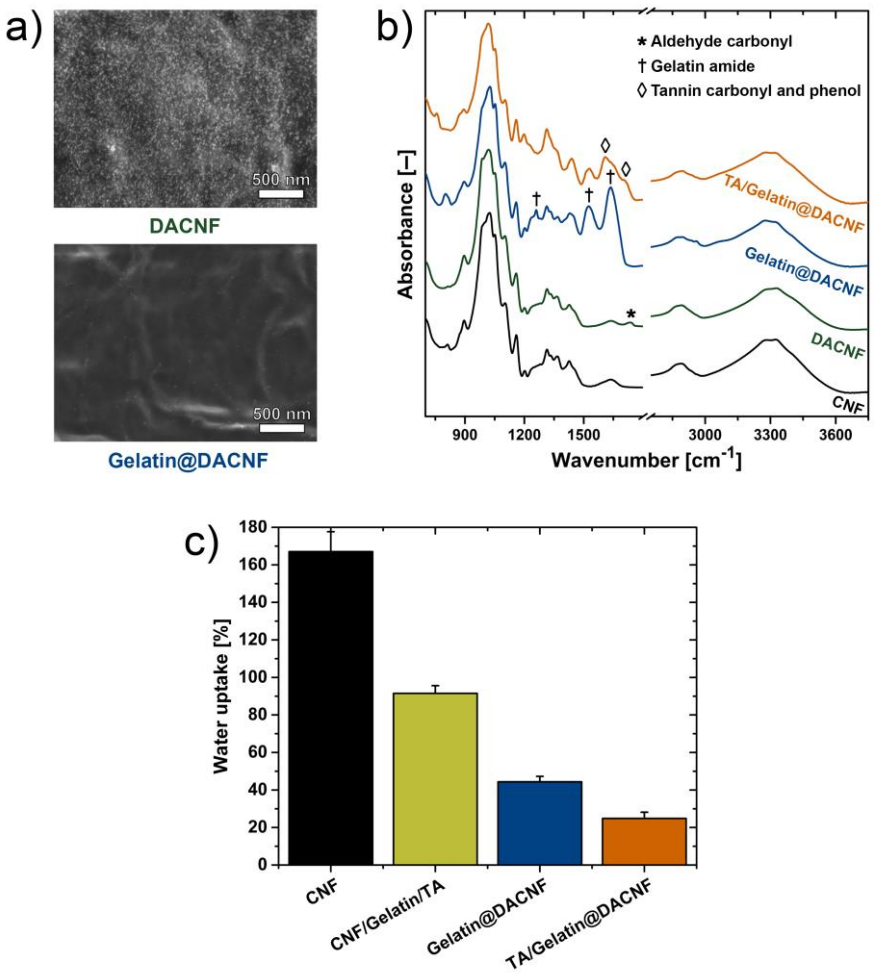

Figure 3.2. Characterization of hybrid films: (a) SEM images of DACNF and gelatin-grafted Gelatin@DACNF films after exposure to diamminesilver(I) (Tollens' reagent); (b) FT-IR spectra and; (c) water uptake of CNF-based hybrid films. Adapted from paper I.[101] © 2020, Biomacromolecules.

3.2. Wet and dry mechanical properties

The mechanical performance of the CNF-based hybrid films was investigated using tensile testing in the dry state after conditioning the specimens at 23 °C and 50% RH for at least 24 hours, and in the wet state after immersing the specimens in DI water, simulated seawater (pH 8.2), or a SDS/TEA solution for one hour. The wet thickness of the films was calculated by multiplying the dry thickness with a swelling ratio, which was obtained from optical microscopy images.

In the dry state, the CNF-based hybrid films show a steep initial elastic region that is followed by a linear plastic deformation regime (Figure 3.3a). The neat CNF films reach a strain at failure of 15.5 ± 2.5% at a tensile strength of 139 ± 9 MPa with a Young's modulus of 4.4 ± 0.3 GPa. The dry leather-inspired TA/Gelatin@DACNF films could not reach the same strain to failure (11.4 ± 1.6%), but had a superior tensile strength (140 ± 12 MPa) and Young's modulus (4.7 ± 0.2 GPa).

Wet films of neat CNF and CNF/Gelatin became very weak as their tensile strength and Young's modulus dropped by over 99%, and failure occurred at low strains of 6.7 ± 1.0% and 7.2 ± 0.8%, respectively (Figure 3.3b). Both, the formation of gelatin-TA complexes in CNF/Gelatin/TA films and interfibril hemiacetal linkages in DACNF films improved the wet mechanical performance with an increase in wet tensile strength of about 3 and 11 times, respectively. Wet gelatin-grafted Gelatin@DACNF and TA/Gelatin@DACNF films show strain hardening during tension, which is assigned to strain-induced fibril alignment.[87] The alignment can be observed by a high degree of birefringence when placing film strips between crossed polarizers at a 45° angle after testing (Figure 3.3b, inset). The wet leather-inspired TA/Gelatin@DACNF hybrid films displayed the by far best mechanical performance (Figure 4.4c–d), which was assigned to strong but flexible interfibrillar cross-links formed by insoluble gelatin-TA complexes. The Young's modulus of 312 ± 26 MPa, tensile strength of 33 ± 2 MPa, strain at failure of 22 ± 2%, and toughness of 3.4 ± 0.4 MJ m^{-3} for these films in the wet state are superior than or comparable to dry bio- and paper-based food packaging materials,[106,107] commercial biodegradable poly(lactic-acid)-based films,[108] and conventional multilayer or LDPE packaging films.[109,110]

The leather-inspired reinforcement could be reversed by the disintegration of the gelatin-TA complexes in an aqueous SDS/TEA solution.[111] The tensile strength and Young's modulus of SDS/TEA-treated films was lower, but the strain at failure similar compared to Gelatin@DACNF, suggesting that the gelatin grafting was not affected (Figure 3.3c–d). Soaking in simulated seawater at pH 8.2 did not significantly deteriorate the wet mechanical properties of the leather-inspired TA/Gelatin@DACNF hybrid films, indicating that the gelatin-TA complexes could withstand high ionic strength and slightly alkaline conditions (Figure 3.3c–d).

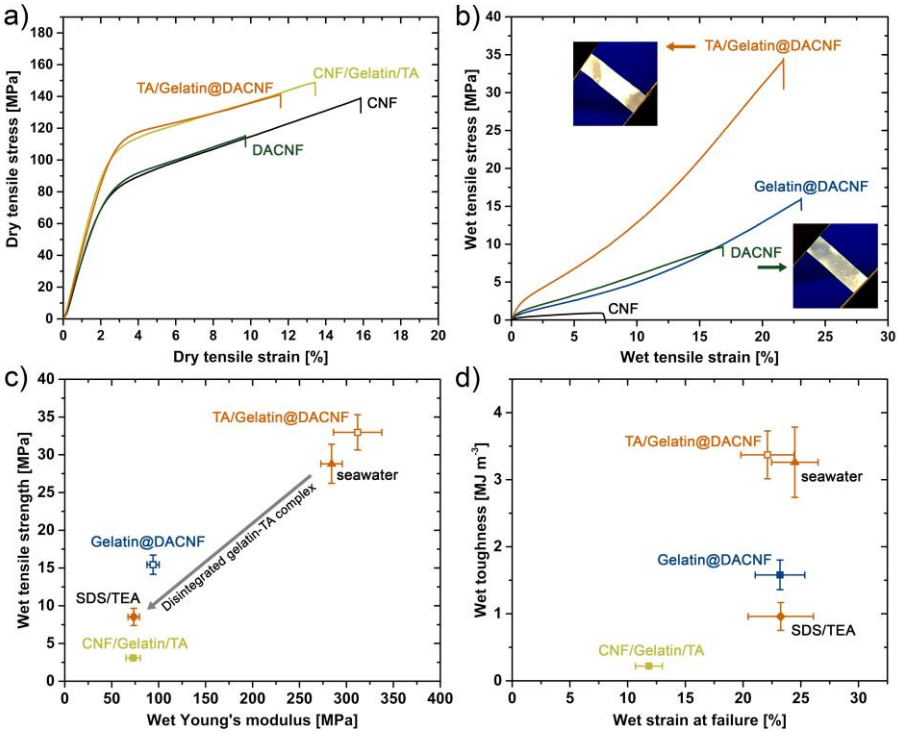

Figure 3.3. Mechanical properties of CNF-based hybrid films: Representative stress–strain curves from tensile testing of (a) dry and (b) wet specimens with (inset) images of DACNF and leather-inspired TA/Gelatin@DACNF film strips placed between crossed polarizers at a 45° angle after testing. Results from wet mechanical testing plotted as; (c) tensile strength vs. Young's modulus and (d) toughness vs. strain at failure. Adapted from paper I.[101] © 2020, Biomacromolecules.

3.3. Antioxidant and UV-blocking properties

The antioxidant activity of the CNF-based hybrid films was assessed using a DPPH assay, in which the absorbance at 517 nm of a colored DPPH free radical solution is measured. Immersing the tannin-containing TA/Gelatin@DACNF films changes the color of the solution from violet to colorless, scavenging more than 94% of the DPPH radicals after only 5 min (Figure 3.4a). Cationic CNF films with a similar tannin content (10 wt%) scavenged only 31% DPPH radicals after 30 min, showing that the leather-inspired TA/Gelatin@DACNF reduced radicals more efficiently.[66] CNF and Gelatin@DACNF films that did not contain tannin scavenged only 3 and 5% of radicals, respectively, after 5 hours.

In addition to scavenging radicals, the conjugated polyphenolic structure of tannins also absorbs harmful UV light from solar radiation in plants.[71] Thus, the UV-blocking capabilities of the CNF-based hybrid films were evaluated using UV-Vis spectroscopy (Figure 3.4b). The ~50 μm thick leather-inspired TA/Gelatin@DACNF films absorbed 100% of UV-B/UV-C light (200–315 nm) and about 88% of UV-A light (315–400 nm). In contrast, the CNF, DACNF, and Gelatin@DACNF films that were not treated with a solution of TA absorbed only between 78 and 80% UV-A, 84 and 86% UV-B, and 94 and 97% UV-C light, respectively. The absorbance of visible light was about 70% in all films, resulting in translucent films (Figure 3.4c). The difference in UV-C light absorbance was demonstrated by irradiating neat CNF and leather-inspired TA/Gelatin@DACNF films with a 254 nm lamp. The tannin-containing films blocked the incoming UV-C light more efficiently, resulting in an opaque material, whereas the neat CNF films remained translucent.

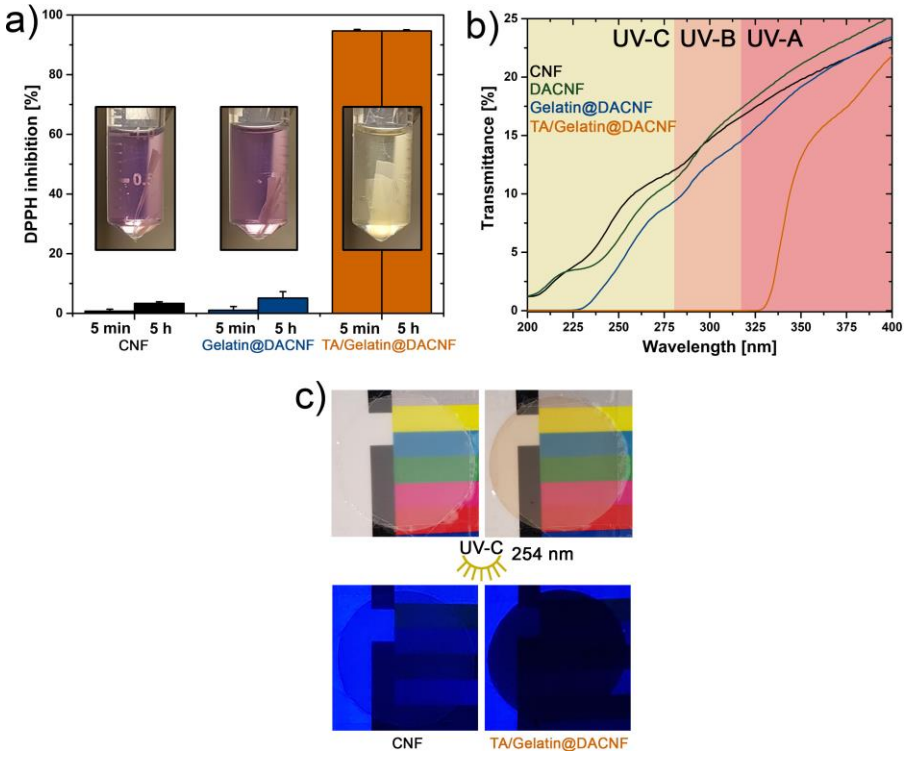

Figure 3.4. Antioxidant and UV-blocking properties of CNF-based hybrid films: (a) DPPH inhibition of CNF, Gelatin@DACNF and leather-inspired TA/Gelatin@DACNF films with (inset) pictures of the DPPH solutions after 5 hours; (b) UV light transmittance of films as a function of the wavelength; (c) Neat CNF and leather-inspired TA/Gelatin@DACNF films before and during irradiation with 254 nm UV-C light. Adapted from paper I.[101] © 2020, Biomacromolecules.

4 Quinone tanning processing of moisture stable foams (Paper II)

In order to enable energy-efficient and scalable evaporative drying of CNF-based porous materials, the CNF network needs to be strengthened enough to withstand structural collapse during drying. Sclerotization, or quinone tanning, is a natural strategy used for example in arthropod cuticles and squid beaks to stabilize and harden materials using covalent cross-links between nucleophilic groups, such as amino groups, and quinones.[112,113] This catecholamine chemistry has been used, for example, to prepare chitin/chitosan films[114–116] and hydrogels.[117,118]

Inspired by sclerotization, we cross-linked ice-templated bPEI-stabilized CNF to form networks that could be evaporatively dried (paper II). The structure is strengthened by non-covalent interactions between CNF and bPEI and by covalent bonds that form via a Michael-type addition reaction of oxidized tannin and bPEI amines. The resulting lightweight and anisotropic biobased foams displayed excellent mechanical and thermal insulation properties at different relative humidities.

4.1. Sclerotization-inspired preparation and characterization of foams

The synthesis of the sclerotization-inspired foams began in an aqueous suspension of 5 mg mL^{-1} carboxylated CNF and 0.5 mg mL^{-1} bPEI, where the partly positively charged polyamine bPEI adsorbs onto the negatively charged CNF (Figure 4.1a). Directional ice-templating of the mixture in a freeze-casting mold results in an anisotropic frozen structure (Figure 4.1b) that is thawed in an aqueous solution of TA (Figure 4.1c), which has been oxidized with $NaIO_4$ to yield quinones (Figure 4.1d). The quinones can crosslink the bPEI via a reaction similar to sclerotization (Figure 4.1e) and the resulting hydrogel

is subsequently washed and solvent exchanged to ethanol. Upon evaporative-drying and heating in an oven (Figure 4.1f), additional amide bonds are formed between CNF and bPEI (Figure 4.1g). The lightweight brown anisotropic foam that is obtained (Figure 4.1h), retains both the shape and the macroporous honeycomb structure (Figure 4.1i) that were formed during directional ice-templating. Analysis of the Hermans' orientation parameter (f_H) from XRD patterns revealed that the CNF in the sclerotization-inspired, evaporatively dried CNF–bPEI–TA foam's thin cell walls (Figure 4.1j) were as aligned as those in anisotropic freeze-dried foams of neat CNF.

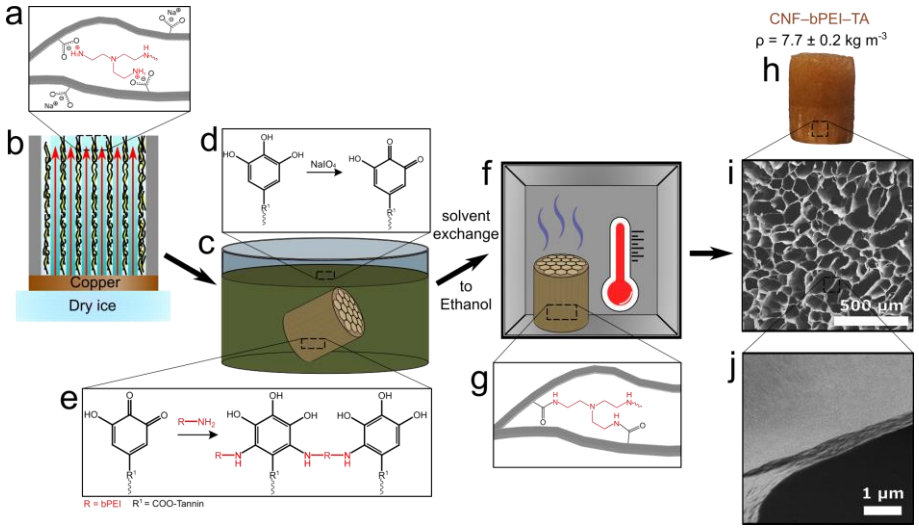

Figure 4.1. Preparation of the sclerotization-inspired CNF–bPEI–TA foams: An aqueous suspension of (a) 5/0.5 mg mL^{-1} CNF/bPEI is (b) ice-templated in a freeze-casting mold and thawed in an (c) aqueous solution of TA, where (d) TA-catechols are formed. (e) The Michael-type cross-linked structure can be (f) evaporatively dried in an oven after solvent exchange to ethanol, where (g) additional cross-links are formed between CNF carboxylates and bPEI amines. SEM images of the (h) CNF–bPEI–TA foam show (i) a macroporous honeycomb structure perpendicular to the freezing direction that consists of (j) thin cell walls. Adapted from paper II.

4.2. Characterization and chemistry of suspensions and foams

The interaction between bPEI and carboxylated CNF leads to aggregation that can be observed from AFM images. The addition of bPEI to CNF with an average diameter of 3.0 ± 0.6 nm leads to the formation of aggregates of entangled CNF/bPEI and excess bPEI with sizes between 60 and 300 nm upon drying (Figure 4.2a). When observing a 5/0.5 mg mL^{-1} CNF/bPEI dispersion between crossed polarizers, the bright areas that indicate ordered CNF domains became smaller suggesting that aggregation between CNF and bPEI prevents CNF assembly (Figure 4.2b).[119] The aggregates in CNF/bPEI suspensions reduce the transmission of visible light slightly with a large drop at shorter wavelengths, suggesting that their size is below 400 nm (Figure 4.2c).[120] The rheological properties of the CNF/bPEI suspension suggest a stronger and more brittle network, as storage and loss modulus increase and the gel breakup occurs more rapidly at lower strains, compared to a neat CNF suspension (Figure 4.2d). Reducing the pH or bPEI concentration in CNF/bPEI suspensions resulted in a more liquid-like behavior.

Lightweight foams were obtained from evaporative drying of ice-templated and solvent-exchanged CNF/bPEI suspensions, either without (CNF–bPEI), or after sclerotization-inspired cross-linking (CNF–bPEI–TA). During the latter, highly reactive electrophilic quinones are formed by oxidizing TA with $NaIO_4$, as demonstrated using UV-Vis spectroscopy (Figure 4.2e), and react with the nucleophilic bPEI amine groups via a Michael-type addition reaction. CNF suspensions did not withstand the capillary forces during evaporative-drying and collapsed; thus neat CNF foams were produced via freeze-drying (CNF–FD) for comparison. The ^{13}C CP-MAS NMR spectrum of the CNF–bPEI–TA foams featured peaks at 138 and 146 ppm, confirming the incorporation of aromatic TA derivatives (Figure 4.2f). In addition, the formation of amide bonds between CNF carboxylates and bPEI amines during oven-drying[121] was verified by the appearance of a peak at 175 ppm in the ^{13}C NMR spectra of CNF–bPEI and CNF–bPEI–TA, and using FT-IR spectroscopy (Figure 4.2g). Sclerotization-inspired cross-linking reduced the absorbance at 570 nm of Ninhydrin solutions that were exposed to the foams by 45%, indicating that the amount of bPEI primary amines decreased after reaction with oxidized tannin (Figure 4.2h).

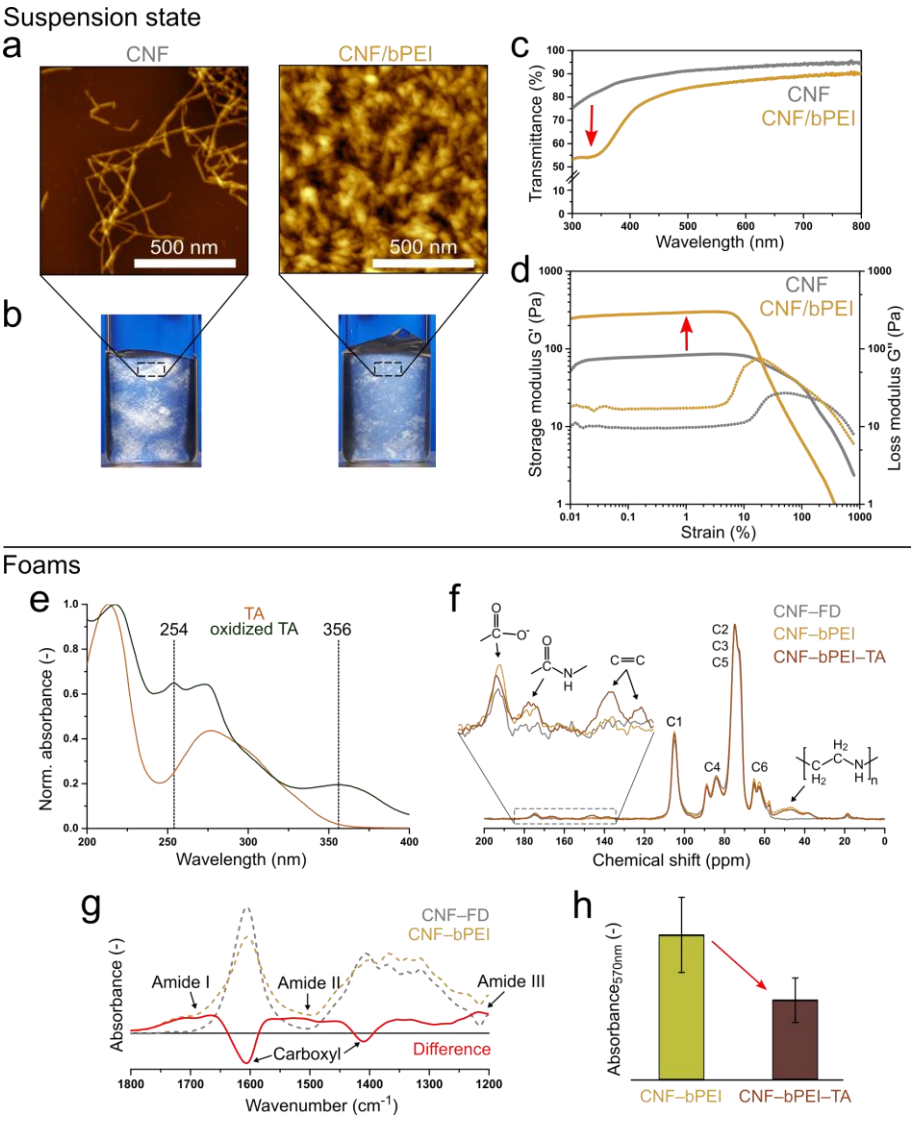

Figure 4.2. Characterization of CNF and CNF/bPEI suspensions and CNF–FD, CNF–bPEI, and CNF–bPEI–TA foams: (a) Topological AFM images; (b) appearance of suspensions between crossed polarizers; (c) UV-Vis transmittance and (d) rheological measurements of suspensions; (e) UV-Vis transmission of oxidized and neat TA solutions; (f) ^{13}C CP-MAS NMR spectra and (g) FT-IR spectra of foams; and (h) absorbance at 570 nm of a Ninhydrin solution after reaction with the foams. Adapted from paper II.

4.3. Moisture stability, mechanical properties and thermal conductivity of foams

The composition, moisture stability, mechanical performance and thermal conductivity of foams at different RH are presented in Table 4.1 and Figure 4.3. The evaporatively dried foams with a CNF content of over 80% had an apparent density as low as 7.7 kg m^{-3} at 50% RH resulting in a porosity of over 99% (Table 4.1). Changing the atmosphere from 50 to 98% RH resulted in a small increase in water uptake and density of the CNF–bPEI–TA foams, whereas non-modified CNF–FD foams absorbed much more moisture and partially collapsed (Figure 4.3a–b).

The mechanical properties in compression were determined along the direction of the cell walls. Sclerotization-inspired cross-linked CNF–bPEI–TA foams exhibited a Young's modulus of 157 ± 40 kPa, a strength of 8.5 ± 0.8 kPa, and a toughness of 8.2 ± 0.5 kJ m^{-3} at 50% RH (Table 4.1). The significantly higher specific Young's modulus of CNF–bPEI–TA compared to CNF–bPEI at 50% and 98% RH shows that the sclerotization-inspired cross-linking stiffens the structure both at moderate and humid conditions (Figure 4.3c). The specific Young's modulus of CNF–bPEI–TA of 20.4 kNm kg^{-1} at 50% RH is higher than previously reported isotropic evaporatively dried CNF-based foams or aerogels.[52–54] The Young's modulus of CNF–bPEI–TA foams decreased by 43% when increasing the RH from 50 to 98%, which is identical to the previously reported decrease in boric acid cross-linked anisotropic freeze-dried foams after changing the atmosphere from 50 to 85% RH.[39] Reposing the CNF–bPEI–TA foams back to 50% RH after conditioning at 98% RH resulted in a small decrease in Young's modulus (12%), but an increase in strength (10%) and toughness (12%), showing that the mechanical properties could be restored after exposure to high RH (Figure 4.3d).

The thermal conductivity of the anisotropic CNF-based foams with aligned cell walls and CNF is always lower in the radial direction (λ_r), i.e. perpendicularly to the fibril and foam cell wall direction, than in the axial direction (λ_a), resulting in anisotropy ratios (λ_a/λ_r) greater than one (Table 4.1).[122,123] The λ_r of evaporatively dried and moisture-stable CNF–bPEI–TA foams was close to the thermal conductivity of air and relatively insensitive to changes in humidity between 20 and 80% RH (Figure 4.3e). CNF–bPEI–TA foams had,

however, higher λ_r compared to freeze-dried CNF-FD foams, which is assigned to the formation of stronger covalent bonds during the sclerotization-inspired cross-linking that promote heat transfer.[124,125] In comparison, the λ_r of CNF–bPEI–TA foams was considerably lower than that of evaporatively dried CNF/polyoxamer foams[41] and conventional insulation materials such as traditional cellulose insulation, fossil-based EPS/XPS foams and mineral wool, but similar to PU foam and higher than super-insulating silica aerogels (Figure 4.3f).[126,127]

Table 4.1. Composition, mechanical properties and thermal conductivity of CNF–FD, CNF–bPEI, and CNF–bPEI–TA foams.

	CNF–FD	CNF–bPEI	CNF–bPEI–TA
Drying method	Freeze-dried	Evaporatively dried	
Composition: CNF/bPEI/TA (wt%)	100	90.9 / 9.1	82.9 / 8.3 / 8.8
Mechanical properties at 50% RH			
Apparent density (kg m^{-3})	6.5 ± 0.1	7.7 ± 0.2	7.7 ± 0.2
Porosity (%)	99.6	99.5	99.5
Young's modulus (kPa)	270 ± 97	98 ± 20	157 ± 40
Strength (kPa)	9.1 ± 0.8	5.8 ± 0.9	8.5 ± 0.8
Toughness (kJ m^{-3})	8.0 ± 0.9	7.2 ± 0.5	8.2 ± 0.5
Mechanical properties at 98% RH			
Shrinkage (vol%)	57 ± 12	10 ± 6	11 ± 3
Apparent density (kg m^{-3})	28.4 ± 16.5	10.7 ± 0.7	10.1 ± 0.4
Porosity (%)	98.1	99.2	99.3
Young's modulus (kPa)	–	32 ± 6	90 ± 16
Strength (kPa)	–	2.1 ± 0.2	4.7 ± 0.6
Toughness (kJ m^{-3})	–	4.0 ± 0.5	6.2 ± 0.5
Thermal conductivity at 50% RH			
λ_r (mW $m^{-1}K^{-1}$)	22.3 ± 0.7	–	26.1 ± 1.0
λ_a (mW $m^{-1}K^{-1}$)	112.3 ± 3.5	–	104.5 ± 5.0
Anisotropy ratio λ_a/λ_r	5.0 ± 0.2	–	4.0 ± 0.3
Thermal conductivity at 80% RH			
λ_r (mW $m^{-1}K^{-1}$)	25.5 ± 0.4	–	26.9 ± 0.3
λ_a (mW $m^{-1}K^{-1}$)	156.0 ± 3.6	–	142.1 ± 3.1
Anisotropy ratio λ_a/λ_r	6.1 ± 0.2	–	5.3 ± 0.1

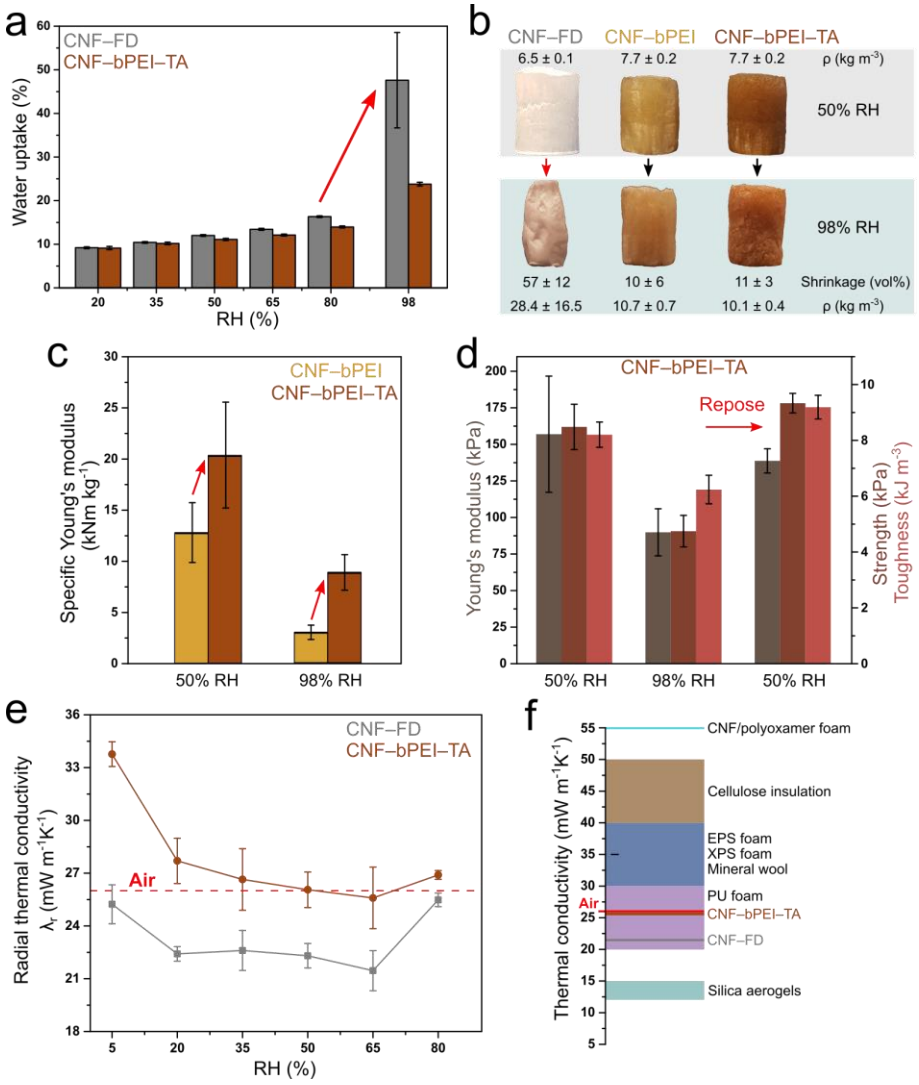

Figure 4.3. Moisture stability, mechanical properties and thermal conductivity of foams: (a) water uptake as a function of RH; (b) influence of high RH on foam structures; (c) specific Young's modulus before and after sclerotization-inspired cross-linking; (d) mechanical properties of CNF–bPEI–TA foams after exposure to high RH; (e) λ_r as a function of RH; (f) Comparison of λ_r to conventional thermal insulation, evaporatively dried CNF-based foams and silica aerogels. Adapted from paper II.

5 Functionalization and patterning of films by complexes of tannins and multivalent metal ions (Paper III)

Accessible organic and inorganic materials have been used to dye and pattern textiles and paper by ancient civilizations around the globe, including Indigo of Woad in Europe,[128] Maya blue in Mesoamerica,[129] and Egyptian pigments in Africa.[130] Black or dark blue dyes that are formed in the reaction between an organic tannin and an inorganic iron salt appeared in European, African, and Asian cultures.[131–134] The coloring principle of these so-called iron-gall inks relies on the formation of dark and insoluble ferric tannate complexes.[75] In Malian culture, *Bògòlanfini* mud cloth is prepared by a unique two-step dyeing technique, where hydrolyzable tannins are pre-adsorbed onto cotton fabric by soaking it in a leaf extract and then patterned using iron-rich mud.[135–137] Apart from its use in printing and traditional dyeing, patterning of cellulose-based substrates has recently been suggested for advanced applications such as bioassays,[138] electroanalytical devices,[139] and wearable electronics.[140]

We used a *Bògòlanfini*-inspired process to pattern and functionalize CNF films with plant-derived hydrolyzable tannins and Earth-abundant metal ions (paper III). Self-standing functionalized CNF-tannin films were prepared and tunable patterns were formed with metal ion solutions using microcontact printing.

The evaporative casting of suspensions containing carboxylated CNF, a hydrolyzable tannin (TA, GA, or EA), and an iron salt ($FeCl_3$, $FeCl_2$, or $FeSO_4$) resulted in self-standing films that remained dark even after washing (Figure 5.1a). Topographical AFM images show CNF networks in unmodified films (Figure 5.1b,i), whereas the films were decorated with GA assemblies upon GA addition (Figure 5.1b,ii). Adding GA and Fe^{III} to a CNF suspension led to the formation of 20–50 nm big nanoparticles on the dry film surface (Figure 5.1b,iii). UV-Vis spectroscopy of suspensions containing GA and Fe^{III} revealed a broad band ~590 nm that corresponds to a ligand–to–metal charge-transfer (LMCT) band between GA ligands and iron (Figure 5.1c). A weak shoulder at ~390 nm was assigned to the formation of GA quinones by a partial reduction of Fe^{III} to Fe^{II}.[141] XANES and XPS measurements demonstrated that iron was present as both Fe^{III} and Fe^{II}, regardless of which salt was initially used to complex GA. Treating GA-impregnated CNF films with Fe^{III} or Fe^{II} shifted the infrared ν(C=O) band of adsorbed GA from 1686 cm^{-1} to 1707 cm^{-1} and replaced the intense CNF ν(C=O) band at 1598 cm^{-1} with a new band at 1629 cm^{-1} (Figure 5.1d). The complexation of GA with iron is indicated by a decreased absorbance of the phenolic ν(HO–C) band (~1244 cm^{-1}) and new peaks at 1582 cm^{-1} and 1427 cm^{-1} that can be assigned to coordinated COO^- asymmetric and symmetric stretching modes, respectively.[142,143]

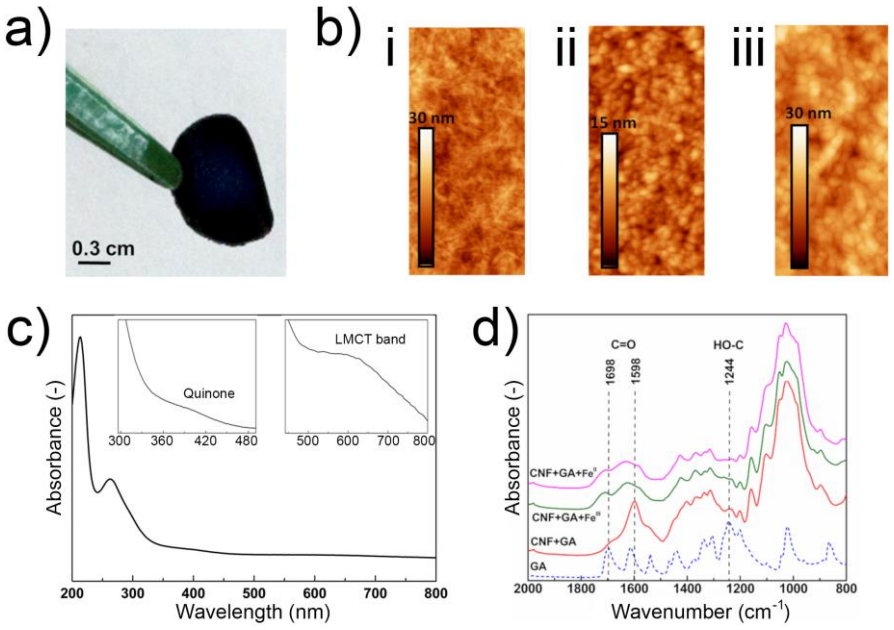

Figure 5.1. Characterization of CNF suspensions and films after modification with GA-Fe$^{II/III}$ complexes: (a) Images of a self-standing film after evaporative casting; (b) Topographical AFM images of (i) a neat CNF film, and films that were treated with (ii) GA and (iii) a mixture of GA and Fe^{III}; (c) UV-Vis spectrum of a CNF+GA+Fe^{III} suspension; (d) IR spectra of films at different stages of the modification. Adapted from paper III.[144] © 2019, Nanoscale.

The ability to decorate CNF films with micron-sized patterns of tannin-iron complexes was demonstrated by microcontact printing. CNF films were evaporative-casted onto a flat silicon substrate and impregnated with a solution of either GA or TA. The pre-adsorbed GA or TA was then locally complexed with a metal salt solution that was inked on a PDMS stamp (Figure 5.2a). Optical microscopy images show that printing with a Fe^{III}-saturated stamp onto a TA-impregnated CNF film results in dark micron-sized line (Figure 5.2b) or dot (Figure 5.2c) patterns that relate to the structure of the printing stamp. Topographical AFM images indicate that the printed lines are 2 µm wide and consist of surface-bound nanoparticles that are ~20 nm in size (Figure 5.2d–f). Back-scattered-electron SEM images of the tannin-iron pattern show bright lines and an EDX Fe-Lα line scan confirms the presence of iron in the lines (Figure 5.2g).

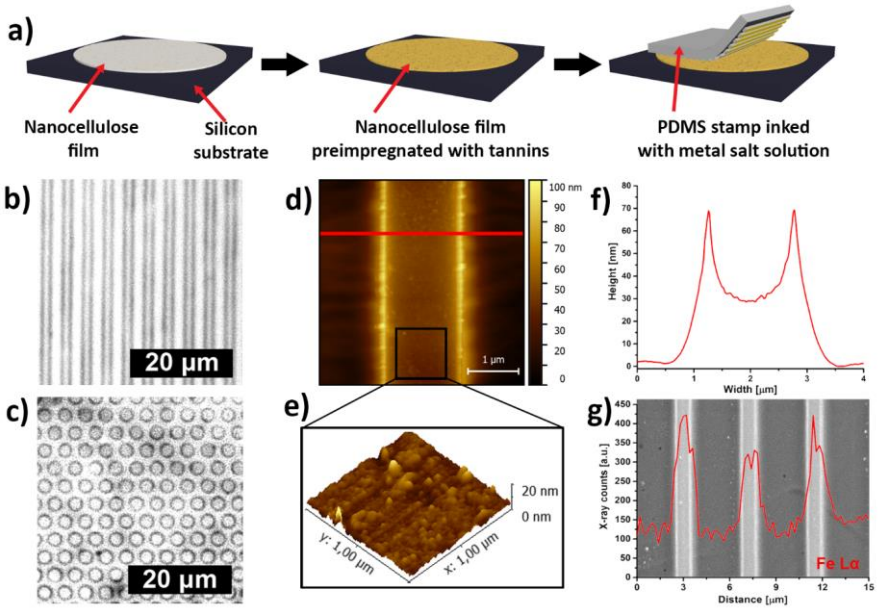

Figure 5.2. Microcontact printing of CNF films with tannin-metal complexes: (a) Illustration of the *Bògòlanfini*-inspired two-step microcontact printing of tannin-impregnated CNF films with metal ion-saturated PDMS stamps; Optical microscopy images of dark micron-sized TA-Fe^{III} (b) line and (c) dot patterns; Tapping-mode AFM images of (d) a single printed TA-Fe^{III} line, (e) a 3D image of the line surface and (f) an extracted height profile across one line; (g) Back-scattered-electron SEM image of a TA-Fe^{III} line pattern including an EDX Fe-Lα line scan. Taken from paper III.[144] © 2019, Nanoscale.

In order to demonstrate that patterning is not limited to TA-Fe^{III} complexes, microcontact printing was also performed on GA-impregnated films using Co^{II} and Cu^{II} salt solutions. Figure 5.3a shows optical microscope images of dark blue GA-Fe^{III}, red GA-Co^{II} and green GA-Cu^{II} line patterns on CNF films. Hence, the color of the created pattern can be easily tuned, by simply changing the metal ion in the printing ink, which results in the formation of metal-catecholate complexes that absorb visible light at different wavelengths.[145]

In addition, the color of Fe^{III}-catechol complexes can be tuned by changing the pH, as the stoichiometry between Fe^{III} and catechol changes from 1:1 at low pH to 1:3 at high pH.[146] Figure 5.3b shows the reversible color change of green acidified TA-Fe^{III} line patterns, to red when the pH was increased, and back to green after acidifying the film surface again. Therefore, complexation of pre-adsorbed tannin with metal ion solutions using microcontact printing constitutes a simple and versatile route towards tunable micron-sized patterns.

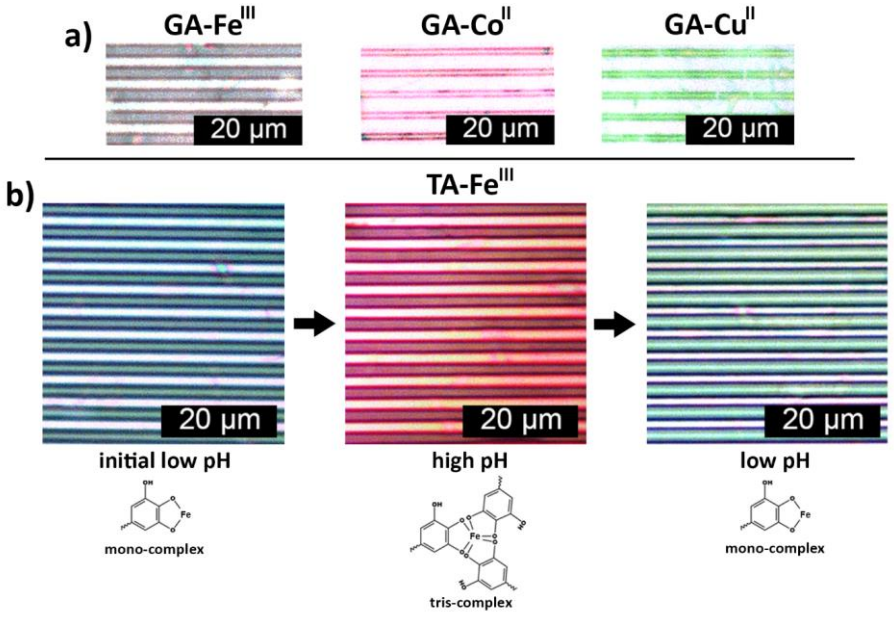

Figure 5.3. Tuning the color of micron-sized patterns on CNF films by modulating the tannin-metal ion complexes: (a) Line patterns of dark GA-Fe^{III}, red GA-Co^{II}, and green GA-Cu^{II} complexes; (b) pH dependent reversible color change of TA-Fe^{III} line patterns. Taken from paper III.[144] © 2019, Nanoscale.

6 Assessment of CNF fibrillation degree by studying anisotropic foams (Paper V)

Benchmarking the degree of fibrillation and increasing the energy efficiency during its processing are crucial to understanding CNF properties and reducing their cost for a given application. Characterizing the mechanical properties of films produced from different grades of CNF has been suggested as indirect method to complement suspension analysis in the assessment of the CNF fibrillation degree.[70] However, there is no common protocol for film processing and characterization, which can also affect measured film properties.[147]

We assessed the degree of CNF fibrillation by analyzing anisotropic foams that were produced by reliable and reproducible directional ice-templating (paper V). A higher degree of fibrillation and thus more homogeneous CNF suspension yields a more uniform macroporous structure, better mechanical performance, as well as increased alignment of CNF and foam cell walls. The specific energy consumption during fibrillation with a grinder was adjusted to optimize the properties of anisotropic freeze-cast foams.

6.1. Production and characterization of CNF

Specific energy consumption was chosen as the main parameter to control the extent of mechanical fibrillation of Sulfite (S) and Kraft (K) pulp. Three CNF suspensions from each pulp (S1–3, K1–3) were obtained after very low energy input followed by two more homogeneous CNF suspensions at higher energy input (S4–5, K4–5; Figure 6.1a). A larger amount of hemicelluloses in the Kraft pulp led to an increased viscosity of the suspension during fibrillation, which resulted in higher specific energy consumptions per pass through the grinder, compared to Sulfite pulp.[148,149]

SEM images of the suspensions (Figure 6.1b) show that fibrillation started in both pulps already after a single pass through the grinder; however, short intact fibers and microfibril aggregates remained in case of Sulfite pulp (S1). The Kraft pulp disintegrated down to the nanofibril level right away, with almost no intact fibers remaining (K1), and formed a homogeneous suspension of CNF at higher energy input (K3–5) with significantly less remaining microfibrils than in Sulfite pulp suspensions (S3–5). The more efficient fibrillation of the Kraft pulp was assigned to the presence of more hemicelluloses that prevent nanofibril aggregation by hydrogen bonding and electrostatic repulsion.[70,148,149]

The fibril aspect ratio of Kraft and Sulfite pulps and CNF suspensions was determined from sedimentation experiments (Figure 6.1c). The sharp increase in the aspect ratio at early fibrillation stages is assigned to a preferred lateral disintegration, which is consistent with SEM observations. More passes through the grinder increase the probability of transversal fibrillation (i.e. cutting of the fibrils), which leads to a gradual decrease in aspect ratio. Kraft CNF have a higher aspect ratio due to smaller fibril diameters from more homogeneous and efficient fibrillation and the Kraft CNF was selected for assessing the fibrillation quality by investigating the properties of anisotropic foams.

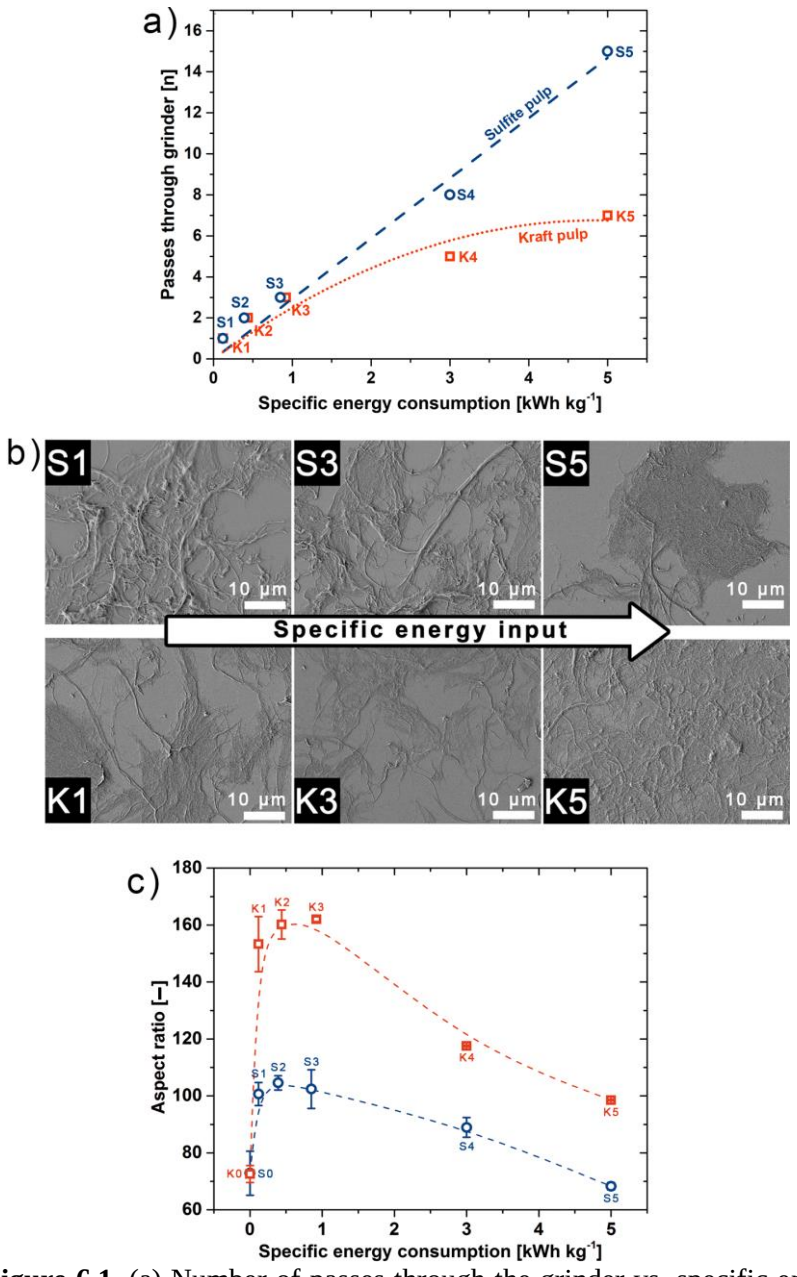

Figure 6.1. (a) Number of passes through the grinder vs. specific energy consumption during fibrillation of Sulfite (○) and Kraft (□) pulp. (b) Morphologies of representative Sulfite (S1–5) and Kraft (K1–5) CNF suspensions produced with increasing energy input. (c) Aspect ratios of fibrillated Sulfite (○) and Kraft (□) pulps as a function of specific energy consumption during fibrillation. Adapted from paper V.[46] © 2020, ACS Sustainable Chem. Eng.

Unidirectional ice-templating and freeze-drying were used to prepare lightweight Kraft pulp (K0) and CNF (K1–5) foams. Figure 6.2 shows representative SEM images of the cross-section of a K0 foam, which lacks any form of defined cellular structure, and of the anisotropic K1–5 CNF foams with aligned columnar macropores. The foams prepared from low-energy-input K1–3 CNF suspensions have defective cell walls and inhomogeneous cell sizes as a consequence of residual macrofibrils and poorly fibrillated material. CNF suspensions produced with a minimum specific energy consumption of 3 kWh kg^{-1} (K4–5) form a more consistent and defined open honeycomb structure with intact cell walls.

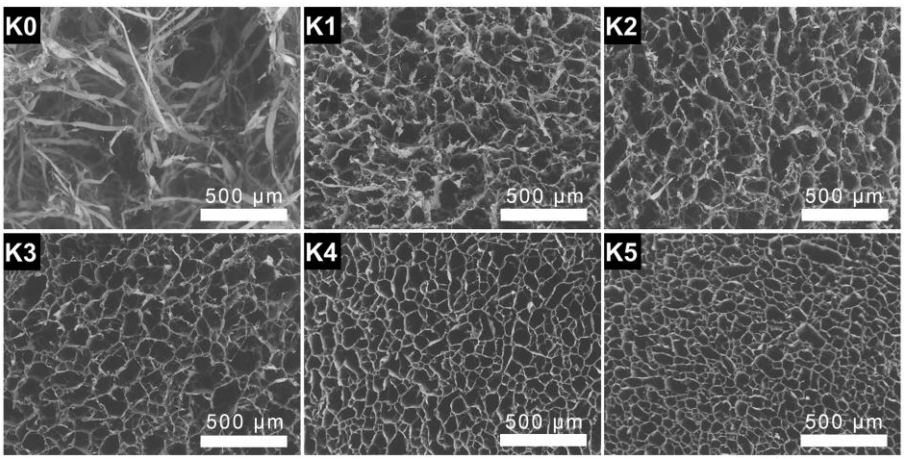

Figure 6.2. SEM images of the cross-section of foams prepared from Kraft pulp (K0) and CNF (K1–5) by ice-templating. Taken from paper V.[46] © 2020, ACS Sustainable Chem. Eng.

The change in macroporous structure of anisotropic foams has a direct influence on their mechanical properties. Both the Young's modulus and energy absorption during compression testing in the axial direction are significantly higher for foams made from K4 CNF compared to foams produced from pulp or low-energy-input CNF. The greater amount of nanofibrils leads to an increase in fibril–fibril bonds that form a tighter and more entangled network which distributes stress more efficiently.[150] The subsequent decrease in modulus combined with an only slight increase in energy absorption suggests that an optimum in specific energy consumption around 3 kWh kg^{-1} could be identified.

6.2. Characterization of CNF and foam cell wall alignment

The CNF and cell wall alignment was quantified by image analysis of SEM images of the axial cross-section of the foams, i.e. along the ice growth direction. Image analysis created color-coded maps from the greyscale SEM images; here, a larger amount of red pixels indicates better alignment in the freezing direction (0°, Figure 6.3a, inset). Figure 6.3a shows the calculated orientation index *f* for the K1–5 foams. The significant increase in *f* between foams prepared from K3 and K4 CNF is in good agreement with the SEM images of the foams radial cross-sections. Additional energy input did not result in better alignment, as *f* did not further increase for K5 foams, suggesting that an optimum around 3 kWh kg^{-1} (K4) could be identified. The Hermans' orientation parameter (f_H) of foams that quantifies CNF crystal unit alignment using XRD ranged from 0.01 (K0) to 0.31 (K5), but did not show a clear trend. Thus, f_H might be useful to compare different types of CNF, but is unreliable for benchmarking the degree of fibrillation.

The thermal conductivity of the CNF foams in the axial (λ_a) and radial (λ_r) directions were measured at 50% relative humidity and 22 °C, and their anisotropy ratios (λ_a/λ_r) were calculated (Figure 6.3b). Increasing energy input during CNF production gave higher λ_a and lower λ_r, and thus higher anisotropy ratios, up to a maximum at a specific energy consumption of 3 kWh kg^{-1}. The tendency towards higher anisotropy ratios is assigned to less defective and more aligned heat-conducting CNF and cell walls and a more uniform porous structure in foams prepared from high energy input CNF.

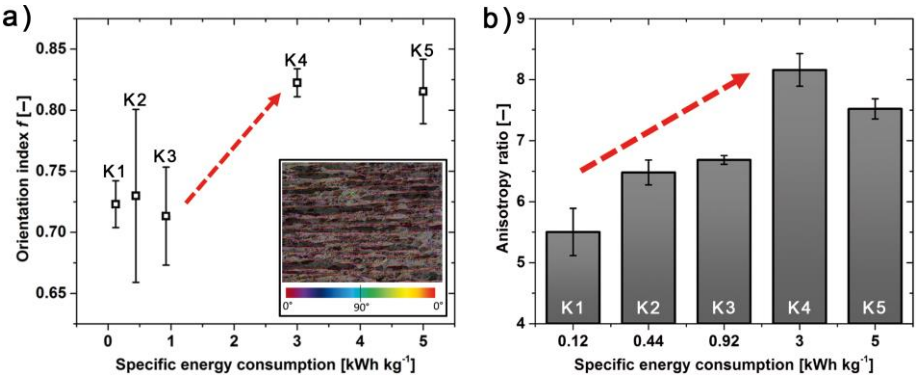

Figure 6.3. Analysis of the CNF and cell wall alignment of K1–5 foams: (a) Orientation index *f* as calculated from the image analysis of SEM images in the axial direction and (b) anisotropy ratio as calculated from dividing the axial by the radial thermal conductivity (λ_a/λ_r). Adapted from paper V.[46] © 2020, ACS Sustainable Chem. Eng.

Overall, the Young's modulus, CNF and cell wall alignment, and anisotropy of thermal conductivity all reached maxima for foams generated from cellulose fibrillated at a specific energy consumption of 3 kWh kg^{-1} (Figure 6.4), suggesting that this energy input yields the highest quality Kraft CNF for the synthesis of anisotropic foams.

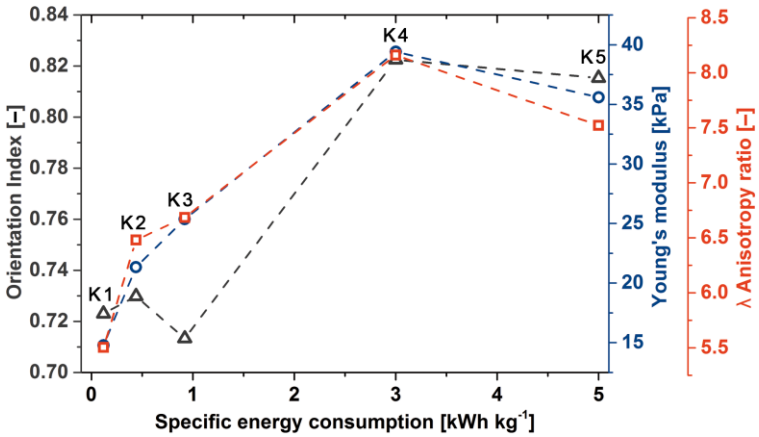

Figure 6.4. Correlation of the orientation index (grey), Young's modulus (blue) and thermal conductivity anisotropy ratio (orange) of foams prepared from K1–5 CNF.

7 Conclusions

In this thesis new potential solutions to key challenges related to the production of CNF and the production and properties of CNF-based films and foams that rely on the physicochemical properties of tannins were presented.

Tannins are defined by their ability to precipitate proteins, a property that was traditionally used to convert animal skins into leather. We mimicked the leather-making process to produce wet-strong CNF-based films by using a tannin to precipitate gelatin that was grafted onto dialdehyde-modified CNF. The wet strength of the leather-inspired films was greater than that of dry plastic films and was assigned to the formation of water-insoluble tannin–gelatin complexes. The polyphenolic tannin provided the film with antioxidant and UV-blocking properties making the multifunctional material a promising renewable alternative to fossil-based food packaging.

The influence of swelling on the accurate measurement and reporting of the wet mechanical properties of CNF-based films and reasons why different approaches exist have been discussed. A set of core recommendations has been presented as a best practice that future studies can use to benchmark wet mechanical performance.

Tannins are rich in catechol groups that can be oxidized to produce quinones that readily react with nucleophilic groups, which is an important step during the sclerotization of insect cuticle. Foams were prepared by a scalable sclerotization-inspired process from suspensions of carboxylated CNF that were aggregated with the polyamine bPEI. The suspensions were ice-templated, cross-linked with an oxidized tannin by a Michael-type reaction, solvent exchanged to ethanol, and evaporatively dried in an oven. Anisotropic, lightweight and moisture-resilient foams were obtained that represent a more sustainable alternative to fossil-based thermal insulation due to their high specific strength and low thermal conductivity at moderate and high RH.

The catechol groups on tannins form colored complexes with multivalent metal ions, such as $Fe^{II/III}$, which is the basis of historic iron gall inks and the traditional *Bògòlanfini* dyeing technique. We used this chemistry to produce micron-sized patterns on CNF films that were pre-impregnated with a tannin. The patterning was performed by microcontact printing using a stamp that was saturated with an aqueous iron salt solution. The color of the patterns could be tuned by changing the pH or the metal ion, illustrating the versatility of this process, which is based solely on renewable and Earth-abundant materials.

The degree of CNF fibrillation was studied with respect to the energy consumption during mechanical grinding of Kraft and Sulfite pulps. CNF suspension analysis showed that the Kraft pulp disintegrated into a more homogeneous material, which was related to the presence of residual hemicelluloses. Anisotropic Kraft CNF foams were produced and their porous structure, CNF and cell wall alignment, mechanical properties, and thermal conductivity were characterized. An optimal energy input of 3 kWh kg^{-1} during CNF production was identified with respect to the CNF foams properties representing a straightforward approach to energy-efficient CNF production.

8 Outlook

The large-scale production and potential commercial application of the leather-inspired films or of a biobased material that exploits similar interactions would be very interesting. One way to reduce the cost of the film could be to replace highly fibrillated CNF with a lower-grade microfibrillated cellulose and commercial tannic acid with a bark extract that is rich in tannins. The animal-derived gelatin could be substituted with industrially produced methylcellulose that also precipitates with tannin. The interactions between gelatin/methylcellulose and tannin could be tuned by the choice of tannin/bark extract towards even better wet and dry mechanical properties. The resulting film should also be further characterized towards potential application as packaging material by e.g. testing its barrier properties and biodegradability.

In addition to fellow students that will hopefully benefit from the proposed best practice on how to measure and report wet mechanical properties of nanocellulose-based materials, the recommendations could also be included in internationally agreed standards to avoid future misunderstandings.

It would be extremely interesting to try to scale up the production of the sclerotized CNF-based foams towards large panels that could be used as thermal insulation in buildings. Since the bottleneck of freeze- or supercritical-drying has been eliminated, the next step could be to find a more efficient alternative to dry ice for the ice-templating. Also, a biobased polyamine could be used to replace fossil-derived bPEI to render the material 100% biobased and the sclerotization-inspired chemistry should be applied to strengthen CNF-based materials other than foams.

The *Bògòlanfini*-inspired microcontact printing on CNF films relies entirely on Earth-abundant, non-toxic, and relatively cheap components, which makes it exciting to try to apply this material as single-use biosensor.

Finally, the suggested approach for correlating the degree of fibrillation to the properties of anisotropic foams needs to be tested on many more types of starting materials and fibrillation methods.

Populärvetenskaplig sammanfattning

Sedan början av 1900-talet har icke förnybara material som t.ex. syntetisk petroleumbaserad plast förändrat vårt samhälle. Med tanke på de miljöproblem som orsakas av plastens långsamma nedbrytning och behovet att radikalt minska användningen av fossila bränslen är det absolut nödvändigt att ersätta icke förnybara material med nya, biologiskt nedbrytbara material som är baserade på förnybara råvaror. Cellulosa, den vanligaste biopolymeren på Jorden och ett traditionellt viktigt råmaterial för industriell produktion av allt ifrån papper till byggmaterial, uppfyller dessa krav. I växter samlas cellulosans molekylkedjor till nanometerstora, kristallina enheter som hålls samman av vätebindningar och bildar cellulosa nanofibrer (CNF). Tillsammans med lignin och hemicelluloser ger dessa motståndskraftiga fibrer växterna sin styrka och stabilitet. CNF kan extraheras från cellulosainnehållande råvaror, såsom pappersmassa, med hjälp av mekaniska och/eller kemiska metoder och är på grund av sina unika egenskaper intressanta byggstenar för produktion av förnybara högpresterande material. CNF har hög specifik styrka och styvhet samt en stor specifik yta som kan modifieras kemiskt. Dessutom är CNF giftfri och biologiskt nedbrytbar, har låg densitet och termisk expansion. En annan grupp av förnybara biomolekyler är polyfenoliska tanniner, vilka ackumuleras av växter som försvarssubstanser i deras bark och löv. Tanniner, som är den näst vanligaste aromatiska biomolekylen efter lignin, har använts som ett garvmedel i tusentals år och ger vissa viner dess strävhet.

Denna avhandling presenterar potentiella lösningar för hur CNF-baserade material med goda egenskaper kan framställas. Först presenteras två strategier som minimerar försvagningen av hydrofila CNF-filmer/-skum i fuktiga och/eller våta förhållanden. I den första delen (kapitel 3, baserad på manuskript I) görs CNF-filmer våtstarka med en läderinspirerad metod som utnyttjar tanniners förmåga att tvärbinda proteiner. CNF modifierades först med gelatin för att producera en film som sedan behandlas med en tannin-

innehållande vattenlösning. Det resulterande materialet besitter såväl en hög våtstyrka som antioxidant och UV-absorberande egenskaper. Oklarheten i hur att draghållfastheten för våta nanocellulosabaserade material skall mätas och rapporterats har analyserats och resulterat i specifika rekommendationer för rapportering av de mekaniska egenskaperna hos dessa material i framtiden (kapitel 2.4.3, baserat på manuskript IV).

Den andra delen av avhandlingen (kapitel 4, baserad på manuskript II) inspirerades av insekters sklerotiserade exoskelett och använder egenskapen hos oxiderade tanniner att reagera med nukleofila grupper. Denna förmåga har användts för att tvärbinda aminmodifierade CNF-skum och öka deras motståndskraft mot vatten. De anisotropa och lätta skummen är mekaniskt stabila och termiskt isolerande vid hög luftfuktighet. Det nya materialet kan också torkas i en konventionell ugn och kräver inte energiintensiv frys- eller superkritisk torkning. I det tredje avsnittet av avhandlingen (kapitel 5, baserat på manuskript III) används tanninkatekolgruppernas förmåga att bilda färgade komplex med järnjoner – liknande den traditionella *Bògòlanfini*-trycktekniken från Mali – för att trycka mikrometerstora och förändringsbara mönster på CNF-filmer. Den nya mönstertekniken använder nästan uteslutande förnybara komponenter samt enkla behandlingsmetoder. Den sista delen av arbetet (kapitel 6, baserat på manuskript V) introducerar en ny metod för att utvärdera och optimisera energieffektiviteten för CNF-produktion genom att utvärdera CNF-fibrilleringsnivån baserat på egenskaperna hos anisotropa skum.

Populärwissenschaftliche Zusammenfassung

Seit Beginn des 20. Jahrhunderts haben nichterneuerbare Materialien, wie etwa synthetische erdöl-basierte Kunststoffe, unsere Gesellschaft grundlegend verändert. In Anbetracht der enormen Umweltverschmutzung durch deren langsame Zersetzung und dem Schwinden fossiler Rohstoffe ist es jedoch unerlässlich, nichterneuerbare Materialien durch neue zu ersetzen – solche, die auf nachwachsenden Rohstoffen basieren und biologisch abbaubar sind. Cellulose – dieses am häufigsten vorkommende Biopolymer und ein traditionell wichtiger Rohstoff für die industrielle Herstellung nachhaltiger Materialien, erfüllt diese Anforderungen. In Pflanzen assemblieren die Cellulosemolekülketten zu nanometerdicken, kristallinen Einheiten die durch Wasserstoffbrückenbindungen zusammengehalten werden und Cellulose-Nanofasern (CNF) bilden. Zusammen mit Lignin und Hemicellulosen verleihen diese reißfesten Fasern den Pflanzen ihre Stärke und Stabilität. CNF können mit mechanischen und/oder chemischen Methoden aus cellulosehaltigen Rohstoffen, wie etwa Zellstoff, extrahiert werden und sind aufgrund ihrer einzigartigen Eigenschaften interessante Bausteine für die Herstellung von erneuerbaren Hochleistungswerkstoffen. Sie besitzen eine hohe spezifische Festigkeit und Steifigkeit, und eine große spezifische Oberfläche, welche chemisch modifizierbar ist. Zusätzlich sind sie ungiftig und biologisch abbaubar, und weisen eine geringe Dichte und Wärmeausdehnung auf. Eine weitere Gruppe von nachwachsenden Biomolekülen sind polyphenole Tannine, die von Pflanzen als Abwehrstoffe in deren Rinde und Blättern angehäuft werden. Tannine sind das zweithäufigste aromatische Biomolekül nach Lignin, finden seit Jahrtausenden Verwendung als Gerbstoff und geben z.B. bestimmten Weinen ihre adstringierende Note.

Diese Dissertation präsentiert potentielle Lösungen zu verbleibenden Herausvorderungen CNF-basierter Materialien. Zunächst werden zwei Strategien vorgestellt, welche die Schwächung von hydrophilen CNF-Filmen/-Schäumen in feuchten und/oder nassen Verhältnissen minimieren. Im

ersten Teil (Kapitel 3, basierend auf Manuskript I) werden CNF-Filme mit einer Leder-inspirierten Methode nassstark gemacht. Hierbei wird die Fähigkeit der Tannine ausgenutzt, Proteine vernetzen zu können. Die CNF werden zunächst mit Gelatine modifiziert und damit ein Film produziert, der danach mit einer wässrigen Tanninlösung behandelt wird. Das entstandene Material ist nun nicht nur reißfest – trocken und nass – sondern besitzt auch antioxidative und UV-absorbierende Fähigkeiten. Unklarheiten hinsichtlich der Messung und Protokollierung der Zugfestigkeit von nassen Nanocellulose-basierten Materialien wurden analysiert und eine Reihe an Empfehlungen werden vorgeschlagen, die dazu beitragen sollen die mechanischen Eigenschaften dieser Materialien in Zukunft besser vergleichen zu können (Kapitel 2.4.3, basierend auf Manuskript IV).

Der zweite Teil der Dissertation (Kapitel 4, basierend auf Manuskript II) wurde inspiriert von sklerotisierten Exoskeletten von Insekten und nutzt die Eigenschaft oxidierter Tannine, mit nukleophilen Gruppen zu reagieren. Diese Fähigkeit wird dazu genutzt um Amin-modifizierte CNF-Schäume zu vernetzen und deren Widerstandsfähigkeit gegen Wasser zu erhöhen. Die anisotropen und leichtgewichtigen Schäume sind dadurch bei hoher Luftfeuchtigkeit mechanisch stabil und wärmeisolierend. Das neue Material kann zudem in einem herkömmlichen Ofen getrocknet werden und benötigt keine energieaufwändige Gefrier- oder überkritische Trocknung. Im dritten Abschnitt der Dissertation (Kapitel 5, basierend auf Manuskript III) wird die Fähigkeit der Tannin-Catecholgruppen mit Eisenionen gefärbte Komplexverbindungen einzugehen – ähnlich wie bei der traditionellen *Bògòlanfini* Drucktechnik aus Mali – dazu benutzt, mikrometerkleine und veränderbare Muster auf CNF-Filme zu drucken. Die neue Drucktechnik benutzt fast ausschließlich nachwachsende und ungefährliche Komponenten und einfache Verarbeitungsmethoden. Der letzte Abschnitt der Arbeit (Kapitel 6, basierend auf Manuskript V) stellt eine neue Methode vor, um die Energieeffizienz während der CNF Herstellung zu optimisieren durch die Evaluierung des CNF Fibrillierungsgrades anhand der Eigenschaften anisotroper Schäume.

Acknowledgements

The last four year of pursuing a PhD degree were not always easy, but highly rewarding in the end. I could never have gotten this far without the constant support and contributions of the following people, which I would like to express my sincere gratitude to:

My supervisor Lennart: Thank you for believing in me and accepting me as a PhD student. I enjoyed working with you and your support and guidance throughout the years made me more confident as a person and scientist. I am very grateful for your help on deciding which ideas were worth proceeding and what was a waste of time. I know that your generosity to send your students to learn and network at conferences all over the world is very unique. Finally, I really enjoyed your lessons on fishing and skiing.

My co-supervisor Aji: Thank you for always having an open door for me and never hesitating to help with scientific questions or experiments in the lab. Also, I am very grateful for a once in a lifetime experience at the conference in Kochi.

My researcher role model Nathalie: Thank you for sharing your immense scientific knowledge on nanocellulose, both in theory and in the lab. You inspired me as a project leader and I am very lucky to have worked with you.

My Master's thesis supervisors Korneliya and Christina: Thanks for being excellent teachers and for giving me such a warm welcome to the group and the department. Not to forget Martin and Miriam, whose exceptional supervision gave me the confidence to study in Sweden in the first place.

The Swedish research council for sustainable development (FORMAS) and Stockholm University for financial support.

My friend Martin: Thanks for being an amazing colleague and neighbor. Your reliable knowledge on many matters helped me a lot throughout my PhD. Also, thanks for organizing our great trip to Peru.

My closest colleagues and friends Vera and Pierre: Thank you for being there for me during my entire PhD journey, in the good and the bad times, by either just listening to my complaints or through great scientific collaborations.

My office mate Tamara: Thank you for the best scientific and non-scientific discussions we had in the office, while mushroom picking or in the climbing

gardens. Also, I am very grateful for all the proof reading and writing science lessons you gave me.

The new generation of PhD students: Ehsan, thank you for your IT support and Persian cooking. Carina, thank you and Hannes for hosting great parties and BBQs. I hope both of you enjoy your time as PhD students as much as I did. Good luck!

All the (former) members of the Bergström group: Andreas, Andi, Hugo, Yingxin, Daniela, Jens, Karin, Arnaud, Felicitas, Mo, Michiel, Lukasz, Melanie, Aygul, Bernd, Veit, Zhong Peng. You made it enjoyable going to work every morning and to discuss over some beers at GV.

Das Genie Micha: Danke für alles, von deiner organisatorischen Hilfe am Anfang, über die tollen Nachmittage und Abende mit deiner liebenswerten Familie, bis hin zu deiner Hilfe beim Umzug.

My guide to Sweden Fredrik: You probably taught me the most about Swedish (drinking) culture and how to correctly perform exercises in the gym. Thank you for being such a loyal friend and mentor.

My student Maria: I was lucky to have worked with such a smart and talented student. You made supervising feel easy.

The helpful MMK professors and scientists: Gunnar, Lars, Cheuk-Wai, Mats, Jiayin, Arnold, James, Adam. Thank you Zoltan, Jekabs, and Kjell for your education and support on the spectroscopy, thermal analysis, and microscopy instruments. Niklas, I am very grateful for your patience when talking Swedish to me and the scientific discussions we had. Mika, thanks for sharing your knowledge on Innebandy and lignin. German, thank you for taking your time to answer my (stupid) questions in such a friendly manner.

The great MMK administrative and technical staff: Camilla, Tatiana, Daniel, Zesi, Ann, Lilian, Christer, Elisabeth, Rolf, Karin, Karim, Pelle, and Jakob you were always patient and ready to help when it was needed. Special thanks to Helmi who assisted me in so many different ways, I don't even know where to start. Anne thank you for a good collaboration during my time as a lab host and in the work environment group.

My fellow PhD council members: Paulo (the greatest chairman), Steffi (the greatest vice-chairman), Alisa, Laura, Olivier, it was a pleasure working with you towards a better student life.

Friends and colleagues at the department: Vahid (the best Innebandy player and philosopher), Xia (thank you for the great Asian restaurant recommendations), Brando (best Italian Dodgeball player), Dimitrios, Anthony, Luis, Yulia, Aditya, Przemek, Hani, Natalia, Jedrzej, Andrea, Blanca, Jinqin, Atefeh, Sadaf, Sugam, Irina, Misha, Fredrik, Frédéric, Miao, Valentina, Ken, Tetyana, Mylad, Jon, Manuel, Florian, Erik, Chuantao, Wenming, Wassilios,

Jianhong, Jian, Dickson, Adrian, Mo, Sahar, Aleksander, Viktor, Mirva, José, Chris, Rihards, Daniel, Maria.

The Innebandy team: Oskar, Jonas, Petr, Baltzar, Mats, Karl. Thank you for making me train my cardio, at least once a week.

All my Stockholm friends: Oscar&Olga, Anne-Liv, Daniel&Åsa, Bob&Marika, Will&Anja, Panos, Agnes&Tiago. You are responsible for me not wanting to move away from this city that feels like home now. Thank you for all the great memories and moments we shared.

A special shout-out to the members of SDA/DS: Marcus, Markus, Henric, Linda, Nathalie&Jordan, Antwone, Happy, Twan, Ben&Elin, Gustav, Frida, Mohsen, Bettan, Klara, Pete&Jannika, Robin, Sebban, Eric, Viggo, Mats and the rest of the dodgeball family. Training, competing, travelling, and celebrating with you is life. Tjoff!

The Solenbergs: Matilda, Elin, Moa, Anna and Johan. Thank you for giving me (literally) a home in Sweden when I arrived and for the delicious dinners.

Meine Freunde aus Österreich: Amelie&Peter, Brabi&Liesi, Liti&Bea, Clemi&Dani, Norbi&Pia, Alex&Babsi, Tomsch, Alex&Anna, Kremsi, Mario&Sabrina, und der Rest der Freundesfreunde. Danke, dass ihr den Kontakt mit mir aufrecht gehalten habt und ich mich immer bei euch melden kann.

I can’t even express how grateful I am to my family, who has always provided me with unconditional love and support. Even in my most egoistic moments you never asked for anything in return. Mama&Papa, danke dass ihr mir ermöglicht habt in Schweden zu studieren und mich zu dem gemacht habt, der ich heute bin. Ohne eure Hilfe wäre all dies nicht möglich gewesen. Karo&Stefan, danke dass ihr immer für mich und Mama&Papa da seit. Emil, ich hoffe dass ich bald wieder mehr Zeit mit dir verbringen kann. Bussi von deinem Onkel. Meinen Großeltern möchte ich für ihre Weisheiten und Geborgenheit danken, sowie dem Rest meiner Familie für die Gewissheit, dass ihr immer für mich da seit.

Linnéa, thank you for your immense love and support during the last (almost) three years. You put up with me in my most stressed and insecure moments and made everything so much easier. Being with you made me a better person and Dodgeball player. Not to forget your lovely family, that I really enjoy spending time with. I am very lucky to have met you. Jag älskar dig! ♥

References

(1) PlasticsEurope. *Plastics – the Facts 2019*; 2019.

(2) Browne, M. A.; Galloway, T.; Thompson, R. Microplastic—an Emerging Contaminant of Potential Concern? *Integr. Environ. Assess. Manag.* **2007**, *3* (4), 559–561. https://doi.org/10.1002/ieam.5630030412.

(3) European Parliament Press Room. Parliament seals ban on throwaway plastics by 2021 https://www.europarl.europa.eu/news/en/press-room/20190321IPR32111/parliament-seals-ban-on-throwaway-plastics-by-2021.

(4) Klemm, D.; Heublein, B.; Fink, H.-P.; Bohn, A. Cellulose: Fascinating Biopolymer and Sustainable Raw Material. *Angew. Chemie Int. Ed.* **2005**, *44* (22), 3358–3393. https://doi.org/10.1002/anie.200460587.

(5) Habibi, Y.; Lucia, L. A.; Rojas, O. J. Cellulose Nanocrystals: Chemistry, Self-Assembly, and Applications. *Chem. Rev.* **2010**, *110* (6), 3479–3500. https://doi.org/10.1021/cr900339w.

(6) Lagerwall, J. P. F.; Schütz, C.; Salajkova, M.; Noh, J.; Hyun Park, J.; Scalia, G.; Bergström, L. Cellulose Nanocrystal-Based Materials: From Liquid Crystal Self-Assembly and Glass Formation to Multifunctional Thin Films. *NPG Asia Mater.* **2014**, *6* (1), e80–e80. https://doi.org/10.1038/am.2013.69.

(7) Lavoine, N.; Desloges, I.; Dufresne, A.; Bras, J. Microfibrillated Cellulose – Its Barrier Properties and Applications in Cellulosic Materials: A Review. *Carbohydr. Polym.* **2012**, *90* (2), 735–764. https://doi.org/10.1016/j.carbpol.2012.05.026.

(8) Pettersen, R. C. The Chemical Composition of Wood. In *The Chemistry of Solid Wood*; Advances in Chemistry; American Chemical Society, 1984; Vol. 207, pp 2–57. https://doi.org/10.1021/ba-1984-0207.ch002.

(9) Rånby, B. G. Fibrous Macromolecular Systems. Cellulose and Muscle. The Colloidal Properties of Cellulose Micelles. *Discuss. Faraday Soc.* **1951**, *11*, 158–164.

(10) Turbak, A. F.; Snyder, F. W.; Sandberg, K. R. Microfibrillated Cellulose, a New Cellulose Product: Properties, Uses, and Commercial Potential. In *J. Appl. Polym. Sci.: Appl. Polym. Symp.;(United States)*; 1983; Vol. 37.

(11) Jonoobi, M.; Oladi, R.; Davoudpour, Y.; Oksman, K.; Dufresne, A.; Hamzeh, Y.; Davoodi, R. Different Preparation Methods and Properties of Nanostructured Cellulose from Various Natural Resources and Residues: A Review. *Cellulose* **2015**, *22* (2), 935–969. https://doi.org/10.1007/s10570-015-0551-0.

(12) Jonoobi, M.; Mathew, A. P.; Oksman, K. Producing Low-Cost Cellulose Nanofiber from Sludge as New Source of Raw Materials. *Ind. Crops Prod.* **2012**, *40*, 232–238. https://doi.org/10.1016/j.indcrop.2012.03.018.

(13) Moon, R. J.; Martini, A.; Nairn, J.; Simonsen, J.; Youngblood, J. Cellulose Nanomaterials Review: Structure, Properties and Nanocomposites. *Chem. Soc. Rev.* **2011**, *40* (7), 3941–3994. https://doi.org/10.1039/C0CS00108B.

(14) Isogai, A.; Saito, T.; Fukuzumi, H. TEMPO-Oxidized Cellulose Nanofibers. *Nanoscale* **2011**, *3* (1), 71–85. https://doi.org/10.1039/c0nr00583e.

(15) Siró, I.; Plackett, D.; Hedenqvist, M.; Ankerfors, M.; Lindström, T. Highly Transparent Films from Carboxymethylated Microfibrillated Cellulose: The Effect of Multiple Homogenization Steps on Key Properties. *J. Appl. Polym. Sci.* **2011**, *119* (5), 2652–2660. https://doi.org/10.1002/app.32831.

(16) Pei, A.; Butchosa, N.; Berglund, L. A.; Zhou, Q. Surface Quaternized Cellulose Nanofibrils with High Water Absorbency and Adsorption Capacity for Anionic Dyes. *Soft Matter* **2013**, *9* (6), 2047–2055. https://doi.org/10.1039/C2SM27344F.

(17) Henschen, J.; Li, D.; Ek, M. Preparation of Cellulose Nanomaterials via Cellulose Oxalates. *Carbohydr. Polym.* **2019**, *213*, 208–216. https://doi.org/https://doi.org/10.1016/j.carbpol.2019.02.056.

(18) Henriksson, M.; Henriksson, G.; Berglund, L. A.; Lindström, T. An Environmentally Friendly Method for Enzyme-Assisted Preparation of Microfibrillated Cellulose (MFC) Nanofibers. *Eur. Polym. J.* **2007**, *43* (8), 3434–3441. https://doi.org/10.1016/j.eurpolymj.2007.05.038.

(19) Li, Q.; McGinnis, S.; Sydnor, C.; Wong, A.; Renneckar, S. Nanocellulose Life Cycle Assessment. *ACS Sustain. Chem. Eng.* **2013**, *1* (8), 919–928. https://doi.org/10.1021/sc4000225.

(20) Arvidsson, R.; Nguyen, D.; Svanström, M. Life Cycle Assessment of Cellulose Nanofibrils Production by Mechanical Treatment and Two Different Pretreatment Processes. *Environ. Sci. Technol.* **2015**, *49* (11), 6881–6890. https://doi.org/10.1021/acs.est.5b00888.

(21) Nechyporchuk, O.; Belgacem, M. N.; Bras, J. Production of Cellulose Nanofibrils: A Review of Recent Advances. *Ind. Crops Prod.* **2016**, *93*, 2–25. https://doi.org/10.1016/j.indcrop.2016.02.016.

(22) Rajinipriya, M.; Nagalakshmaiah, M.; Robert, M.; Elkoun, S. Importance of Agricultural and Industrial Waste in the Field of Nanocellulose and Recent Industrial Developments of Wood Based Nanocellulose: A Review. *ACS Sustain. Chem. Eng.* **2018**, *6* (3), 2807–2828. https://doi.org/10.1021/acssuschemeng.7b03437.

(23) marketsandmarkets.com. *Nanocellulose Market by Type (MFC & NFC, CNC/NCC, and Others), Application (Pulp&paper, Composites, Biomedical & Pharmaceutical, Electronics & Sensors, and Others), Region (Europe, North America, APAC, and Rest of World) - Global Forecast to 2025*; 2020.

(24) Benítez, A. J.; Walther, A. Cellulose Nanofibril Nanopapers and Bioinspired Nanocomposites: A Review to Understand the Mechanical Property Space. *J. Mater. Chem. A* **2017**, *5* (31), 16003–16024. https://doi.org/10.1039/c7ta02006f.

(25) Daicho, K.; Kobayashi, K.; Fujisawa, S.; Saito, T. Crystallinity-Independent yet Modification-Dependent True Density of Nanocellulose. *Biomacromolecules* **2020**, *21* (2), 939–945. https://doi.org/10.1021/acs.biomac.9b01584.

(26) Guan, Q.-F.; Yang, H.-B.; Han, Z.-M.; Zhou, L.-C.; Zhu, Y.-B.; Ling, Z.-C.; Jiang, H.-B.; Wang, P.-F.; Ma, T.; Wu, H.-A.; et al. Lightweight, Tough, and Sustainable Cellulose Nanofiber-Derived Bulk Structural Materials with Low Thermal Expansion Coefficient. *Sci. Adv.* **2020**, *6* (18), eaaz1114. https://doi.org/10.1126/sciadv.aaz1114.

(27) Abitbol, T.; Rivkin, A.; Cao, Y.; Nevo, Y.; Abraham, E.; Ben-Shalom, T.; Lapidot, S.; Shoseyov, O. Nanocellulose, a Tiny Fiber with Huge Applications. *Curr. Opin. Biotechnol.* **2016**, *39*, 76–88. https://doi.org/10.1016/j.copbio.2016.01.002.

(28) Dufresne, A. *Nanocellulose - From Nature to High Performance Tailored Materials*, 2. Edition.; De Gruyter: Berlin, Boston, 2018. https://doi.org/10.1515/9783110254600.

(29) Lee, K.-Y.; Aitomäki, Y.; Berglund, L. A.; Oksman, K.; Bismarck, A. On the Use of Nanocellulose as Reinforcement in Polymer Matrix Composites. *Compos. Sci. Technol.* **2014**, *105*, 15–27. https://doi.org/10.1016/j.compscitech.2014.08.032.

(30) Niinivaara, E.; Cranston, E. D. Bottom-up Assembly of Nanocellulose Structures. *Carbohydr. Polym.* **2020**, *247*, 116664. https://doi.org/10.1016/j.carbpol.2020.116664.

(31) Dufresne, A. Nanocellulose: A New Ageless Bionanomaterial. *Mater. Today* **2013**, *16* (6), 220–227. https://doi.org/10.1016/j.mattod.2013.06.004.

(32) Ferrer, A.; Pal, L.; Hubbe, M. Nanocellulose in Packaging: Advances in Barrier Layer Technologies. *Ind. Crops Prod.* **2017**, *95*, 574–582. https://doi.org/10.1016/j.indcrop.2016.11.012.

(33) Hubbe, M. A.; Ferrer, A.; Tyagi, P.; Yin, Y.; Salas, C.; Pal, L.; Rojas, O. J. Nanocellulose in Thin Films, Coatings, and Plies for Packaging Applications: A Review. *BioResources* **2017**, *12* (1), 2143–2233.

(34) Li, F.; Mascheroni, E.; Piergiovanni, L. The Potential of Nanocellulose in the Packaging Field: A Review. *Packag. Technol. Sci.* **2015**, *28* (6), 475–508. https://doi.org/10.1002/pts.2121.

(35) Voisin, H.; Bergström, L.; Liu, P.; Mathew, A. Nanocellulose-Based Materials for Water Purification. *Nanomaterials* **2017**, *7* (3), 57. https://doi.org/10.3390/nano7030057.

(36) Lavoine, N.; Bergström, L. Nanocellulose-Based Foams and Aerogels: Processing, Properties, and Applications. *J. Mater. Chem. A* **2017**, *5* (31), 16105–16117. https://doi.org/10.1039/C7TA02807E.

(37) Kobayashi, Y.; Saito, T.; Isogai, A. Aerogels with 3D Ordered Nanofiber Skeletons of Liquid-Crystalline Nanocellulose Derivatives as Tough and Transparent Insulators. *Angew. Chemie Int. Ed.* **2014**, *53* (39), 10394–10397. https://doi.org/10.1002/anie.201405123.

(38) Chen, W.; Li, Q.; Wang, Y.; Yi, X.; Zeng, J.; Yu, H.; Liu, Y.; Li, J. Comparative Study of Aerogels Obtained from Differently Prepared Nanocellulose Fibers. *ChemSusChem* **2014**, *7* (1), 154–161. https://doi.org/10.1002/cssc.201300950.

(39) Wicklein, B.; Kocjan, A.; Salazar-Alvarez, G.; Carosio, F.; Camino, G.; Antonietti, M.; Bergström, L. Thermally Insulating and Fire-Retardant Lightweight Anisotropic Foams Based on Nanocellulose and Graphene Oxide. *Nat. Nanotechnol.* **2015**, *10*, 277–283. https://doi.org/10.1038/nnano.2014.248.

(40) Benítez, A. J.; Torres-Rendon, J.; Poutanen, M.; Walther, A. Humidity and Multiscale Structure Govern Mechanical Properties and Deformation Modes in Films of Native Cellulose Nanofibrils. *Biomacromolecules* **2013**, *14* (12), 4497–4506. https://doi.org/10.1021/bm401451m.

(41) Apostolopoulou-Kalkavoura, V.; Gordeyeva, K.; Lavoine, N.; Bergström, L. Thermal Conductivity of Hygroscopic Foams Based on Cellulose Nanofibrils and a Nonionic Polyoxamer. *Cellulose* **2018**, *25* (2), 1117–1126. https://doi.org/10.1007/s10570-017-1633-y.

(42) Sjöstedt, A.; Wohlert, J.; Larsson, P. T.; Wågberg, L. Structural Changes during Swelling of Highly Charged Cellulose Fibres. *Cellulose* **2015**, *22* (5), 2943–2953.

https://doi.org/10.1007/s10570-015-0701-4.

(43) Aulin, C.; Ahola, S.; Josefsson, P.; Nishino, T.; Hirose, Y.; Osterberg, M.; Wagberg, L. Nanoscale Cellulose Films with Different Crystallinities and Mesostructures-Their Surface Properties and Interaction with Water. *Langmuir* **2009**, *25* (13), 7675–7685.

(44) Liang, L.; Bhagia, S.; Li, M.; Huang, C.; Ragauskas, A. J. Cross-Linked Nanocellulosic Materials and Their Applications. *ChemSusChem* **2020**, *13* (1), 78–87. https://doi.org/10.1002/cssc.201901676.

(45) Walther, A.; Lossada, F.; Benselfelt, T.; Kriechbaum, K.; Berglund, L.; Ikkala, O.; Saito, T.; Wågberg, L.; Bergström, L. Best Practice for Reporting Wet Mechanical Properties of Nanocellulose-Based Materials. *Biomacromolecules* **2020**. https://doi.org/10.1021/acs.biomac.0c00330.

(46) Kriechbaum, K.; Munier, P.; Apostolopoulou-Kalkavoura, V.; Lavoine, N. Analysis of the Porous Architecture and Properties of Anisotropic Nanocellulose Foams: A Novel Approach to Assess the Quality of Cellulose Nanofibrils (CNFs). *ACS Sustain. Chem. Eng.* **2018**, *6* (9), 11959–11967. https://doi.org/10.1021/acssuschemeng.8b02278.

(47) Munier, P.; Apostolopoulou-Kalkavoura, V.; Persson, M.; Bergström, L. Strong Silica-Nanocellulose Anisotropic Composite Foams Combine Low Thermal Conductivity and Low Moisture Uptake. *Cellulose* **2019**, *0*. https://doi.org/10.1007/s10570-019-02912-0.

(48) Peng, Y.; Gardner, D. J.; Han, Y. Drying Cellulose Nanofibrils: In Search of a Suitable Method. *Cellulose* **2012**, *19* (1), 91–102. https://doi.org/10.1007/s10570-011-9630-z.

(49) Ratti, C. Hot Air and Freeze-Drying of High-Value Foods: A Review. *J. Food Eng.* **2001**, *49* (4), 311–319. https://doi.org/10.1016/S0260-8774(00)00228-4.

(50) Gordeyeva, K.; Voisin, H.; Hedin, N.; Bergström, L.; Lavoine, N. Lightweight Foams of Amine-Rich Organosilica and Cellulose Nanofibrils by Foaming and Controlled Condensation of Aminosilane. *Mater. Chem. Front.* **2018**, *2* (12), 2220–2229. https://doi.org/10.1039/c8qm00360b.

(51) Gordeyeva, K. S.; Fall, A. B.; Hall, S.; Wicklein, B.; Bergström, L. Stabilizing Nanocellulose-Nonionic Surfactant Composite Foams by Delayed Ca-Induced Gelation. *J. Colloid Interface Sci.* **2016**, *472*, 44–51. https://doi.org/10.1016/j.jcis.2016.03.031.

(52) Françon, H.; Wang, Z.; Marais, A.; Mystek, K.; Piper, A.; Granberg, H.; Malti, A.; Gatenholm, P.; Larsson, P. A.; Wågberg, L. Ambient-Dried , 3D-Printable and Electrically Conducting Cellulose Nanofiber Aerogels by Inclusion of Functional Polymers. **2020**. https://doi.org/10.1002/adfm.201909383.

(53) Li, Y.; Tanna, V. A.; Zhou, Y.; Winter, H. H.; Watkins, J. J.; Carter, K. R. Nanocellulose Aerogels Inspired by Frozen Tofu. *ACS Sustain. Chem. Eng.* **2017**, *5* (8), 6387–6391. https://doi.org/10.1021/acssuschemeng.7b01608.

(54) Erlandsson, J.; Françon, H.; Marais, A.; Granberg, H.; Wågberg, L. Cross-Linked and Shapeable Porous 3D Substrates from Freeze-Linked Cellulose Nanofibrils. *Biomacromolecules* **2018**, acs.biomac.8b01412. https://doi.org/10.1021/acs.biomac.8b01412.

(55) Erlandsson, J.; Pettersson, T.; Ingverud, T.; Granberg, H.; Larsson, P. A.; Malkoch, M.; Wagberg, L. On the Mechanism behind Freezing-Induced Chemical Crosslinking in Ice-Templated Cellulose Nanofibril Aerogels. *J. Mater. Chem. A* **2018**, *6* (40), 19371–19380. https://doi.org/10.1039/C8TA06319B.

(56) Mittal, N.; Jansson, R.; Widhe, M.; Benselfelt, T.; Håkansson, K. M. O.; Lundell, F.; Hedhammar, M.; Söderberg, L. D. Ultrastrong and Bioactive Nanostructured Bio-Based Composites. *ACS Nano* **2017**, *11* (5), 5148–5159. https://doi.org/10.1021/acsnano.7b02305.

(57) Toivonen, M. S.; Kurki-Suonio, S.; Schacher, F. H.; Hietala, S.; Rojas, O. J.; Ikkala, O. Water-Resistant, Transparent Hybrid Nanopaper by Physical Cross-Linking with Chitosan. *Biomacromolecules* **2015**, *16* (3), 1062–1071. https://doi.org/10.1021/acs.biomac.5b00145.

(58) Benselfelt, T.; Engström, J.; Wagberg, L. Supramolecular Double Networks of Cellulose Nanofibrils and Algae Polysaccharides with Excellent Wet Mechanical Properties. *Green Chem.* **2018**, *20* (11), 2558–2570. https://doi.org/10.1039/C8GC00590G.

(59) Mathew, A. P.; Oksman, K.; Pierron, D.; Harmad, M.-F. Crosslinked Fibrous Composites Based on Cellulose Nanofibers and Collagen with in Situ PH Induced Fibrillation. *Cellulose* **2012**, *19* (1), 139–150. https://doi.org/10.1007/s10570-011-9624-x.

(60) Liu, J.; Chinga-Carrasco, G.; Cheng, F.; Xu, W.; Willför, S.; Syverud, K.; Xu, C. Hemicellulose-Reinforced Nanocellulose Hydrogels for Wound Healing Application. *Cellulose* **2016**, *23* (5), 3129–3143. https://doi.org/10.1007/s10570-016-1038-3.

(61) Farooq, M.; Zou, T.; Riviere, G.; Sipponen, M. H.; Österberg, M. Strong, Ductile and Waterproof Cellulose Nanofibril Composite Films with Colloidal Lignin Particles. *Biomacromolecules* **2018**, *20* (2), 693–704. https://doi.org/10.1021/acs.biomac.8b01364.

(62) Krogell, J.; Holmbom, B.; Pranovich, A.; Hemming, J.; Willför, S. Extraction and Chemical Characterization of Norway Spruce Inner and Outer Bark. *Nord Pulp Pap Res J* **2012**, *27* (1), 6–17. https://doi.org/10.3183/npprj-2012-27-01-p006-017.

(63) Li, D.; Moriana, R.; Ek, M. From Forest Residues to Hydrophobic Nanocomposites with High Oxygen-Barrier Properties. *Nord. Pulp Pap. Res. J.* **2016**, *31* (2), 261–269.

(64) Feng, S.; Cheng, S.; Yuan, Z.; Leitch, M.; Xu, C. (Charles). Valorization of Bark for Chemicals and Materials: A Review. *Renew. Sustain. Energy Rev.* **2013**, *26*, 560–578. https://doi.org/10.1016/j.rser.2013.06.024.

(65) Missio, A. L.; Mattos, B. D.; Ferreira, D. de F.; Magalhães, W. L. E.; Bertuol, D. A.; Gatto, D. A.; Petutschnigg, A.; Tondi, G. Nanocellulose-Tannin Films: From Trees to Sustainable Active Packaging. *J. Clean. Prod.* **2018**, *184*, 143–151. https://doi.org/10.1016/j.jclepro.2018.02.205.

(66) Li, P.; Sirviö, J. A.; Haapala, A.; Khakalo, A.; Liimatainen, H. Anti-Oxidative and UV-Absorbing Biohybrid Film of Cellulose Nanofibrils and Tannin Extract. *Food Hydrocoll.* **2019**, *92*, 208–2017. https://doi.org/10.1016/j.foodhyd.2019.02.002.

(67) Spence, K. L.; Venditti, R. A.; Rojas, O. J.; Habibi, Y.; Pawlak, J. J. A Comparative Study of Energy Consumption and Physical Properties of Microfibrillated Cellulose Produced by Different Processing Methods. *Cellulose* **2011**, *18* (4), 1097–1111. https://doi.org/10.1007/s10570-011-9533-z.

(68) Chinga-Carrasco, G. Optical Methods for the Quantification of the Fibrillation Degree of Bleached MFC Materials. *Micron* **2013**, *48*, 42–48. https://doi.org/10.1016/j.micron.2013.02.005.

(69) Kangas, H.; Lahtinen, P.; Sneck, A.; Saariaho, A.-M.; Laitinen, O.; Hellén, E. Characterization of Fibrillated Celluloses. A Short Review and Evaluation of

Characteristics with a Combination of Methods. *Nord. Pulp Pap. Res. J.* **2014**, *29* (1), 129–143. https://doi.org/10.3183/npprj-2014-29-01-p129-143.

(70) Desmaisons, J.; Boutonnet, E.; Rueff, M.; Dufresne, A.; Bras, J. A New Quality Index for Benchmarking of Different Cellulose Nanofibrils. *Carbohydr. Polym.* **2017**, *174*, 318–329. https://doi.org/10.1016/j.carbpol.2017.06.032.

(71) Quideau, S.; Deffieux, D.; Douat-Casassus, C.; Pouységu, L. Plant Polyphenols: Chemical Properties, Biological Activities, and Synthesis. *Angew. Chemie - Int. Ed.* **2011**, *50* (3), 586–621. https://doi.org/10.1002/anie.201000044.

(72) Haslam, E. *Plant Polyphenols: Vegetable Tannins Revisited*; CUP Archive, 1989.

(73) Sarni-Manchado, P.; Cheynier, V.; Moutounet, M. Interactions of Grape Seed Tannins with Salivary Proteins. *J. Agric. Food Chem.* **1999**, *47* (1), 42–47. https://doi.org/10.1021/jf9805146.

(74) *Chemistry and Significance of Condensed Tannins*, 1st ed.; Hemingway, R. W., Karchesy, J. J., Branham, S. J., Eds.; Plenum Press, 1989.

(75) Krekel, C. The Chemistry of Historical Iron Gall Inks. *Int J Forensic Doc Exam* **1999**, *5*, 54–58.

(76) Yang, J.; Cohen Stuart, M. A.; Kamperman, M. Jack of All Trades: Versatile Catechol Crosslinking Mechanisms. *Chem. Soc. Rev.* **2014**, *43* (24), 8271–8298. https://doi.org/10.1039/C4CS00185K.

(77) Pizzi, A. Tannins: Major Sources, Properties and Applications. In *Monomers, Polymers and Composites from Renewable Resources*; Belgacem, M. N., Ed.; Elsevier: Amsterdam, 2008; pp 179–199. https://doi.org/10.1016/B978-0-08-045316-3.00008-9.

(78) Saito, T.; Isogai, A. TEMPO-Mediated Oxidation of Native Cellulose. The Effect of Oxidation Conditions on Chemical and Crystal Structures of the Water-Insoluble Fractions. *Biomacromolecules* **2004**, *5* (5), 1983–1989. https://doi.org/10.1021/bm0497769.

(79) Gibson, L. J.; Ashby, M. F. *Cellular Solids: Structure and Properties*; Cambridge University Press, 1999. https://doi.org/10.1017/CBO9781139878326.

(80) Bondet, V.; Brand-Williams, W.; Berset, C. Kinetics and Mechanisms of Antioxidant Activity Using the DPPH. Free Radical Method. *LWT-Food Sci. Technol.* **1997**, *30* (6), 609–615. https://doi.org/10.1006/fstl.1997.0240.

(81) Dash, R.; Foston, M.; Ragauskas, A. J. Improving the Mechanical and Thermal Properties of Gelatin Hydrogels Cross-Linked by Cellulose Nanowhiskers. *Carbohydr. Polym.* **2013**, *91* (2), 638–645. https://doi.org/10.1016/j.carbpol.2012.08.080.

(82) Stryer, L. *Biochemistry*, 3rd ed.; Freeman, 1988.

(83) Varanasi, S.; He, R.; Batchelor, W. Estimation of Cellulose Nanofibre Aspect Ratio from Measurements of Fibre Suspension Gel Point. *Cellulose* **2013**, *20* (4), 1885–1896. https://doi.org/10.1007/s10570-013-9972-9.

(84) Martinez, D. M.; Buckley, K.; Jivan, S.; Lindstrom, A.; Thiruvengadaswamy, R.; Olson, J. A.; Ruth, T. J.; Kerekes, R. J. Characterizing the Mobility of Papermaking Fibres during Sedimentation. In *Proceedings of the Transactions of 12th fundamental Research Symposium, Oxford*; 2001; pp 225–254.

(85) Rezakhaniha, R.; Agianniotis, A.; Schrauwen, J. T. C.; Griffa, A.; Sage, D.; Bouten, C. V. C.; Van De Vosse, F. N.; Unser, M.; Stergiopulos, N. Experimental Investigation

of Collagen Waviness and Orientation in the Arterial Adventitia Using Confocal Laser Scanning Microscopy. *Biomech. Model. Mechanobiol.* **2012**, *11* (3–4), 461–473. https://doi.org/10.1007/s10237-011-0325-z.

(86) Püspöki, Z.; Storath, M.; Sage, D.; Unser, M. Transforms and Operators for Directional Bioimage Analysis: A Survey. In *Focus on Bio-Image Informatics*; Springer, 2016; pp 69–93. https://doi.org/978-3-319-28549-8_3.

(87) Sehaqui, H.; Ezekiel Mushi, N.; Morimune, S.; Salajkova, M.; Nishino, T.; Berglund, L. A. Cellulose Nanofiber Orientation in Nanopaper and Nanocomposites by Cold Drawing. *ACS Appl. Mater. Interfaces* **2012**, *4* (2), 1043–1049. https://doi.org/10.1021/am2016766.

(88) Hermans, J. J.; Hermans, P. H.; Vermaas, D.; Weidinger, A. Quantitative Evaluation of Orientation in Cellulose Fibres from the X-Ray Fibre Diagram. *Recl. des Trav. Chim. des Pays-Bas* **1946**, *65* (6), 427–447. https://doi.org/10.1002/recl.19460650605.

(89) Gelb, L. D.; Gubbinst, K. E. Characterization of Porous Glasses: Simulation Models, Adsorption Isotherms, and the Brunauer-Emmett-Teller Analysis Method. *Langmuir* **1998**, *14* (8), 2097–2111. https://doi.org/10.1021/la9710379.

(90) Nie, B.; Liu, X.; Yang, L.; Meng, J.; Li, X. Pore Structure Characterization of Different Rank Coals Using Gas Adsorption and Scanning Electron Microscopy. *Fuel* **2015**, *158*, 908–917. https://doi.org/10.1016/j.fuel.2015.06.050.

(91) Spoljaric, S.; Salminen, A.; Luong, N. D.; Seppälä, J. Crosslinked Nanofibrillated Cellulose: Poly(Acrylic Acid) Nanocomposite Films; Enhanced Mechanical Performance in Aqueous Environments. *Cellulose* **2013**, *20* (6), 2991–3005. https://doi.org/10.1007/s10570-013-0061-x.

(92) Yang, W.; Bian, H.; Jiao, L.; Wu, W.; Deng, Y.; Dai, H. High Wet-Strength, Thermally Stable and Transparent TEMPO-Oxidized Cellulose Nanofibril Film: Via Cross-Linking with Poly-Amide Epichlorohydrin Resin. *RSC Adv.* **2017**, *7* (50), 31567–31573. https://doi.org/10.1039/c7ra05009g.

(93) Lossada, F.; Guo, J.; Jiao, D.; Groeer, S.; Bourgeat-Lami, E.; Montarnal, D.; Walther, A. Vitrimer Chemistry Meets Cellulose Nanofibrils: Bioinspired Nanopapers with High Water Resistance and Strong Adhesion. *Biomacromolecules* **2019**, *20* (2), 1045–1055. https://doi.org/10.1021/acs.biomac.8b01659.

(94) Hoenders, D.; Guo, J.; Goldmann, A. S.; Barner-Kowollik, C.; Walther, A. Photochemical Ligation Meets Nanocellulose: A Versatile Platform for Self-Reporting Functional Materials. *Mater. Horizons* **2018**, *5* (3), 560–568. https://doi.org/10.1039/c8mh00241j.

(95) Shimizu, M.; Saito, T.; Isogai, A. Water-Resistant and High Oxygen-Barrier Nanocellulose Films with Interfibrillar Cross-Linkages Formed through Multivalent Metal Ions. *J. Memb. Sci.* **2016**, *500*, 1–7. https://doi.org/10.1016/j.memsci.2015.11.002.

(96) Bideau, B.; Bras, J.; Adoui, N.; Loranger, E.; Daneault, C. Polypyrrole/Nanocellulose Composite for Food Preservation: Barrier and Antioxidant Characterization. *Food Packag. Shelf Life* **2017**, *12*, 1–8. https://doi.org/10.1016/j.fpsl.2017.01.007.

(97) Ataide, J. A.; De Carvalho, N. M.; Rebelo, M. D. A.; Chaud, M. V.; Grotto, D.; Gerenutti, M.; Rai, M.; Mazzola, P. G.; Jozala, A. F. Bacterial Nanocellulose Loaded with Bromelain: Assessment of Antimicrobial, Antioxidant and Physical-Chemical Properties. *Sci. Rep.* **2017**, *7* (1), 2–10. https://doi.org/10.1038/s41598-017-18271-4.

(98) Alzate-Arbeláez, A. F.; Dorta, E.; López-Alarcón, C.; Cortés, F. B.; Rojano, B. A.

Immobilization of Andean Berry (Vaccinium Meridionale) Polyphenols on Nanocellulose Isolated from Banana Residues: A Natural Food Additive with Antioxidant Properties. *Food Chem.* **2019**, *294*, 503–517. https://doi.org/10.1016/j.foodchem.2019.05.085.

(99) Hagerman, A. E.; Butler, L. G. The Specificity of Proanthocyanidin-Protein Interactions. *J. Biol. Chem.* **1981**, *256* (9), 4494–4497.

(100) Covington, A. D. Modern Tanning Chemistry. *Chem. Soc. Rev.* **1997**, *26* (2), 111–126. https://doi.org/10.1039/cs9972600111.

(101) Kriechbaum, K.; Bergström, L. Antioxidant and UV-Blocking Leather-Inspired Nanocellulose-Based Films with High Wet Strength. *Biomacromolecules* **2020**. https://doi.org/10.1021/acs.biomac.9b01655.

(102) Wang, Y.; Jiang, L.; Duan, J.; Shao, S. Effect of the Carbonyl Content on the Properties of Composite Films Based on Oxidized Starch and Gelatin. *J. Appl. Polym. Sci.* **2013**, *130* (5), 3809–3815. https://doi.org/10.1002/app.39493.

(103) Kim, U.-J.; Kuga, S.; Wada, M.; Okano, T.; Kondo, T. Periodate Oxidation of Crystalline Cellulose. *Biomacromolecules* **2000**, *1* (3), 488–492. https://doi.org/10.1021/bm0000337.

(104) Le Bourvellec, C.; Renard, C. M. G. C. Interactions between Polyphenols and Macromolecules: Quantification Methods and Mechanisms. *Crit. Rev. Food Sci. Nutr.* **2012**, *52* (3), 213–248. https://doi.org/10.1080/10408398.2010.499808.

(105) Saito, T.; Isogai, A. Introduction of Aldehyde Groups on Surfaces of Native Cellulose Fibers by TEMPO-Mediated Oxidation. *Colloids Surfaces A Physicochem. Eng. Asp.* **2006**, *289* (1–3), 219–225. https://doi.org/10.1016/j.colsurfa.2006.04.038.

(106) Briassoulis, D.; Giannoulis, A. Evaluation of the Functionality of Bio-Based Food Packaging Films. *Polym. Test.* **2018**, *69*, 39–51. https://doi.org/10.1016/j.polymertesting.2018.05.003.

(107) Rhim, J. W. Effect of Moisture Content on Tensile Properties of Paper-Based Food Packaging Materials. *Food Sci. Biotechnol.* **2010**, *19* (1), 243–247. https://doi.org/10.1007/s10068-010-0034-x.

(108) Vanstrom, J. R. Mechanical Characterization of Commercial Biodegradable Plastic Films, 2012, Vol. 12661.

(109) Oliveira, V. M.; Nogueira, B. R.; Ortiz, A. V.; Moura, E. A. B. Mechanical and Thermal Properties of Commercial Multilayer Flexible Plastic Packaging Materials Irradiated with Electron Beam. *Nukleonika* **2008**, *53*, 141–144.

(110) Rennert, M.; Nase, M.; Lach, R.; Reincke, K.; Arndt, S.; Androsch, R.; Grellmann, W. Influence of Low-Density Polyethylene Blown Film Thickness on the Mechanical Properties and Fracture Toughness. *J. Plast. Film Sheeting* **2013**, *29* (4), 327–346. https://doi.org/10.1177/8756087913483751.

(111) Hagerman, A. E.; Butler, L. G. Protein Precipitation Method for the Quantitative Determination of Tannins. *J. Agric. Food Chem.* **1978**, *26* (4), 809–812. https://doi.org/10.1021/jf60218a027.

(112) Andersen, S. O. Insect Cuticular Sclerotization: A Review. *Insect Biochem. Mol. Biol.* **2010**, *40* (3), 166–178. https://doi.org/10.1016/j.ibmb.2009.10.007.

(113) Miserez, A.; Schneberk, T.; Sun, C.; Zok, F. W.; Waite, J. H. The Transition from Stiff to Compliant Materials in Squid Beaks. *Science* **2008**, *319* (5871), 1816–1819. https://doi.org/10.1126/science.1154117.

(114) Ryu, J. H.; Jo, S.; Koh, M. Y.; Lee, H. Bio-Inspired, Water-Soluble to Insoluble Self-Conversion for Flexible, Biocompatible, Transparent, Catecholamine Polysaccharide Thin Films. *Adv. Funct. Mater.* **2014**, *24* (48), 7709–7716. https://doi.org/10.1002/adfm.201402250.

(115) Oh, D. X.; Hwang, D. S. A Biomimetic Chitosan Composite with Improved Mechanical Properties in Wet Conditions. *Biotechnol. Prog.* **2013**, *29* (2), 505–512. https://doi.org/10.1002/btpr.1691.

(116) Zhang, X.; Hassanzadeh, P.; Miyake, T.; Jin, J.; Rolandi, M. Squid Beak Inspired Water Processable Chitosan Composites with Tunable Mechanical Properties. *J. Mater. Chem. B* **2016**, *4* (13), 2273–2279. https://doi.org/10.1039/c6tb00106h.

(117) Chen, C.; Li, D.; Yano, H.; Abe, K. Insect Cuticle-Mimetic Hydrogels with High Mechanical Properties Achieved via the Combination of Chitin Nanofiber and Gelatin. *J. Agric. Food Chem.* **2019**, *67* (19), 5571–5578. https://doi.org/10.1021/acs.jafc.9b00984.

(118) Cho, J. H.; Lee, J. S.; Shin, J.; Jeon, E. J.; An, S.; Choi, Y. S.; Cho, S. W. Ascidian-Inspired Fast-Forming Hydrogel System for Versatile Biomedical Applications: Pyrogallol Chemistry for Dual Modes of Crosslinking Mechanism. *Adv. Funct. Mater.* **2018**, *28* (6), 1–10. https://doi.org/10.1002/adfm.201705244.

(119) Habibi, Y.; Chanzy, H.; Vignon, M. R. TEMPO-Mediated Surface Oxidation of Cellulose Whiskers. *Cellulose* **2006**, *13* (6), 679–687. https://doi.org/10.1007/s10570-006-9075-y.

(120) Saito, T.; Nishiyama, Y.; Putaux, J. L.; Vignon, M.; Isogai, A. Homogeneous Suspensions of Individualized Microfibrils from TEMPO-Catalyzed Oxidation of Native Cellulose. *Biomacromolecules* **2006**, *7* (6), 1687–1691. https://doi.org/10.1021/bm060154s.

(121) Melone, L.; Rossi, B.; Pastori, N.; Panzeri, W.; Mele, A.; Punta, C. TEMPO-Oxidized Cellulose Cross-Linked with Branched Polyethyleneimine: Nanostructured Adsorbent Sponges for Water Remediation. *Chempluschem* **2015**, *80* (9), 1408–1415. https://doi.org/10.1002/cplu.201500145.

(122) Dri, F. L.; Shang, S. L.; Hector, L. G.; Saxe, P.; Liu, Z. K.; Moon, R. J.; Zavattieri, P. D. Anisotropy and Temperature Dependence of Structural, Thermodynamic, and Elastic Properties of Crystalline Cellulose Iβ: A First-Principles Investigation. *Model. Simul. Mater. Sci. Eng.* **2014**, *22* (8). https://doi.org/10.1088/0965-0393/22/8/085012.

(123) Diaz, J. A.; Ye, Z.; Wu, X.; Moore, A. L.; Moon, R. J.; Martini, A.; Boday, D. J.; Youngblood, J. P. Thermal Conductivity in Nanostructured Films: From Single Cellulose Nanocrystals to Bulk Films. *Biomacromolecules* **2014**, *15* (11), 4096–4101. https://doi.org/10.1021/bm501131a.

(124) Losego, M. D.; Grady, M. E.; Sottos, N. R.; Cahill, D. G.; Braun, P. V. Effects of Chemical Bonding on Heat Transport across Interfaces. *Nat. Mater.* **2012**, *11* (6), 502–506. https://doi.org/10.1038/nmat3303.

(125) Kim, G.-H.; Lee, D.; Shanker, A.; Shao, L.; Kwon, M. S.; Gidley, D.; Kim, J.; Pipe, K. P. High Thermal Conductivity in Amorphous Polymer Blends by Engineered Interchain Interactions. *Nat. Mater.* **2015**, *14* (3), 295–300. https://doi.org/10.1038/nmat4141.

(126) Jelle, B. P. Traditional, State-of-the-Art and Future Thermal Building Insulation Materials and Solutions: Properties, Requirements and Possibilities. *Energy Build.* **2011**, *43*, 2549–2563. https://doi.org/10.1016/j.enbuild.2011.05.015.

(127) Budtova, T. Bio-Based Aerogels: A New Generation of Thermal Superinsulating Materials. In *Cellulose Science and Technology: Chemistry, Analysis, and Applications*; John Wiley & Sons: Chichester, UK, 2018; pp 371–392.

(128) Epstein, E.; Nabors, M. W.; Stowe, B. B. Origin of Indigo of Woad. *Nature* **1967**, *216* (5115), 547–549. https://doi.org/10.1038/216547a0.

(129) José-Yacamán, M.; Rendón, L.; Arenas, J.; Puche, M. C. S. Maya Blue Paint: An Ancient Nanostructured Material. *Science* **1996**, *273* (5272), 223 LP – 225. https://doi.org/10.1126/science.273.5272.223.

(130) Ancient Egyptian Pigments 1. *Nature* **1894**, *49* (1268), 374–375. https://doi.org/10.1038/049374a0.

(131) Ye, Y.; Salmon, L. G.; Cass, G. R. The Ozone Fading of Traditional Chinese Plant Dyes. *J. Am. Inst. Conserv.* **2000**, *39* (2), 245–257. https://doi.org/10.1179/019713600806082685.

(132) Eusman, E. Iron gall ink - History https://irongallink.org/igi_index8a92.html (accessed Jun 8, 2020).

(133) Siva, R. Status of Natural Dyes and Dye-Yielding Plants in India. *Curr. Sci.* **2007**, *92* (7), 916–925.

(134) Festa, G.; Christiansen, T.; Turina, V.; Borla, M.; Kelleher, J.; Arcidiacono, L.; Cartechini, L.; Ponterio, R. C.; Scatigno, C.; Senesi, R.; et al. Egyptian Metallic Inks on Textiles from the 15th Century BCE Unravelled by Non-Invasive Techniques and Chemometric Analysis. *Sci. Rep.* **2019**, *9* (1), 7310. https://doi.org/10.1038/s41598-019-43655-z.

(135) Donne, J. B. Bogolanfini: A Mud-Painted Cloth from Mali. *Man* **1973**, *8* (1), 104–107. https://doi.org/10.2307/2800615.

(136) Limaye, M. V; Bacsik, Z.; Schütz, C.; Dembelé, A.; Pléa, M.; Andersson, L.; Salazar-Alvarez, G.; Bergström, L. On the Role of Tannins and Iron in the Bogolan or Mud Cloth Dyeing Process. *Text. Res. J.* **2012**, *82* (18), 1888–1896. https://doi.org/10.1177/0040517512452955.

(137) Imperato, P. J.; Shamir, M. Bokolanfini: Mud Cloth of the Bamana of Mali. *African Arts* **1970**, *3* (4), 32–80. https://doi.org/10.2307/3345905.

(138) Martinez, A. W.; Phillips, S. T.; Butte, M. J.; Whitesides, G. M. Patterned Paper as a Platform for Inexpensive, Low-Volume, Portable Bioassays. *Angew. Chemie Int. Ed.* **2007**, *46* (8), 1318–1320. https://doi.org/10.1002/anie.200603817.

(139) Lan, W.-J.; Maxwell, E. J.; Parolo, C.; Bwambok, D. K.; Subramaniam, A. B.; Whitesides, G. M. Paper-Based Electroanalytical Devices with an Integrated, Stable Reference Electrode. *Lab Chip* **2013**, *13* (20), 4103–4108. https://doi.org/10.1039/C3LC50771H.

(140) Liu, H.; Qing, H.; Li, Z.; Han, Y. L.; Lin, M.; Yang, H.; Li, A.; Lu, T. J.; Li, F.; Xu, F. Paper: A Promising Material for Human-Friendly Functional Wearable Electronics. *Mater. Sci. Eng. R Reports* **2017**, *112*, 1–22. https://doi.org/10.1016/j.mser.2017.01.001.

(141) Tofan-Lazar, J.; Situm, A.; Al-Abadleh, H. A. DRIFTS Studies on the Role of Surface Water in Stabilizing Catechol–Iron(III) Complexes at the Gas/Solid Interface. *J. Phys. Chem. A* **2013**, *117* (40), 10368–10380. https://doi.org/10.1021/jp406113r.

(142) Rahim, M. A.; Kempe, K.; Müllner, M.; Ejima, H.; Ju, Y.; van Koeverden, M. P.; Suma, T.; Braunger, J. A.; Leeming, M. G.; Abrahams, B. F.; et al. Surface-Confined

Amorphous Films from Metal-Coordinated Simple Phenolic Ligands. *Chem. Mater.* **2015**, *27* (16), 5825–5832. https://doi.org/10.1021/acs.chemmater.5b02790.

(143) Guo, J.; Ping, Y.; Ejima, H.; Alt, K.; Meissner, M.; Richardson, J. J.; Yan, Y.; Peter, K.; von Elverfeldt, D.; Hagemeyer, C. E.; et al. Engineering Multifunctional Capsules through the Assembly of Metal–Phenolic Networks. *Angew. Chemie Int. Ed.* **2014**, *53* (22), 5546–5551. https://doi.org/10.1002/anie.201311136.

(144) Limaye, M. V; Schütz, C.; Kriechbaum, K.; Wohlert, J.; Bacsik, Z.; Wohlert, M.; Xia, W.; Pléa, M.; Dembele, C.; Salazar-Alvarez, G.; et al. Functionalization and Patterning of Nanocellulose Films by Surface-Bound Nanoparticles of Hydrolyzable Tannins and Multivalent Metal Ions. *Nanoscale* **2019**, *11* (41), 19278–19284. https://doi.org/10.1039/C9NR04142G.

(145) Sever, M. J.; Wilker, J. J. Visible Absorption Spectra of Metal--Catecholate and Metal--Tironate Complexes. *Dalt. Trans.* **2004**, No. 7, 1061–1072. https://doi.org/10.1039/B315811J.

(146) Ejima, H.; Richardson, J. J.; Liang, K.; Best, J. P.; van Koeverden, M. P.; Such, G. K.; Cui, J.; Caruso, F. One-Step Assembly of Coordination Complexes for Versatile Film and Particle Engineering. *Science* **2013**, *341* (6142), 154–157. https://doi.org/10.1126/science.1237265.

(147) Hervy, M.; Santmarti, A.; Lahtinen, P.; Tammelin, T.; Lee, K.-Y. Sample Geometry Dependency on the Measured Tensile Properties of Cellulose Nanopapers. *Mater. Des.* **2017**, *121*, 421–429. https://doi.org/10.1016/j.matdes.2017.02.081.

(148) Solala, I.; Volperts, A.; Andersone, A.; Dizhbite, T.; Mironova-Ulmane, N.; Vehniäinen, A.; Pere, J.; Vuorinen, T. Mechanoradical Formation and Its Effects on Birch Kraft Pulp during the Preparation of Nanofibrillated Cellulose with Masuko Refining. *Holzforschung* **2012**, *66* (4), 477–483. https://doi.org/10.1515/hf.2011.183.

(149) Iwamoto, S.; Abe, K.; Yano, H. The Effect of Hemicelluloses on Wood Pulp Nanofibrillation and Nanofiber Network Characteristics. *Biomacromolecules* **2008**, *9* (3), 1022–1026. https://doi.org/10.1021/bm701157n.

(150) Dufresne, A.; Cavaille, J.-Y.; Vignon, M. R. Mechanical Behavior of Sheets Prepared from Sugar Beet Cellulose Microfibrils. *J. Appl. Polym. Sci.* **1997**, *64* (6), 1185–1194. https://doi.org/10.1002/(SICI)1097-4628(19970509)64:6%3C1185::AID-APP19%3E3.0.CO;2-V.